SPACE BASED EVALUATION OF THE AEROSOL INDIRECT EFFECT

IN THE ARCTIC

by

Kyle Tietze

A thesis submitted to the faculty of
The University of Utah
in partial fulfillment of the requirements for the degree of

Master of Science

Department of Atmospheric Science

The University of Utah

May 2011

The University of Utah Graduate School

STATEMENT OF THESIS APPROVAL

The thesis of **Kyle Tietze**

has been approved by the following supervisory committee members:

Timothy J. Garrett	, Chair	**11/12/2010** Date Approved
Kevin D. Perry	, Member	**11/12/2010** Date Approved
Gerald G. Mace	, Member	**11/12/2010** Date Approved

and by **W. James Steenburgh** , Chair of the Department of **Mines and Earth Sciences**

and by Charles A. Wight, Dean of The Graduate School.

ABSTRACT

During the Arctic winter and spring, enhanced levels of aerosol particles and trace gases form a pronounced haze originating primarily from industrial pollutants transported into the region. The haze rapidly dissipates during the late spring as pollution transport is inhibited and meteorological conditions favor pollutant removal. Prior ground based studies have found that aerosols associated with the "Arctic haze" have the potential to indirectly alter Arctic cloud surface radiative forcing in both the solar and thermal IR bands. While satellites have been used extensively to study the indirect effects of aerosols on clouds in lower latitude regions, they rarely are employed in Arctic studies. One limitation of using satellites to study aerosols and clouds is that they do not provide retrievals of aerosol concentrations under cloudy conditions nor do they resolve aerosol vertical profiles; co-location of aerosol and cloud fields is therefore impossible. The ubiquitous nature of Arctic clouds makes the common practice of comparing cloud properties to aerosol in nearby cloud free regions a difficult task in the Arctic, providing little information about aerosol-cloud interactions.

Here, in order to circumvent these concerns, passive satellite cloud property retrievals are co-located horizontally, vertically and temporally with pollution tracers from a Lagrangian particle dispersion transport model. The advantage of this analysis approach is that clouds and pollution are compared where they are affected by the same meteorological conditions. This means that pollution can be treated as an independent variable affecting cloud properties. Cloud properties from low level liquid clouds north of 65 °N are co-located with fields of pollution tracer during the period March 20 to July 20, 2008. The analysis shows a high sensitivity of cloud optical depth and droplet effective radius to the

anthropogenic and biomass burning pollution tracers. Furthermore, the cloud sensitivity to pollution is evaluated under different thermodynamic and physical constraints. Results of the analysis show a strong indication of wet-scavenging reducing the effects of pollution on clouds at warmer temperatures. Additionally, the sensitivity to pollution is higher for cloud optical depth than for droplet effective radius, suggesting that some sort of feedback process amplifies the radiative response through changes in liquid water path.

TABLE OF CONTENTS

ACKNOWLEDGMENTS

First and foremost I would like to thank my adviser, Dr. Tim Garrett, for his encouragement, patience, commitment and for providing unique research and travel opportunities which greatly enhanced the education I received. I also extend my thanks to my committee members, Dr Perry and Dr Mace, whom I benefited greatly from being a student in their classrooms and from their insightful comments and suggestions.

A huge thanks goes to Andreas Stohl for providing lots of support with data access and prompt troubleshooting replies. Especially helpful was his expert scientific advise related to the project which he freely offered. I am extremely appreciative of all the support I received from Jérôme Riedi and his endless patience while assisting my research in France and from across the Atlantic Ocean. I also grateful for all the help I received from the staff of Laboratoire d'Optique Atmosphérique during my stay in Lille, France. In particular, Francois Thieuleux who spent many hours getting me up to date with software, data processing and French language.

I thank all my friends in the department for providing an amazing supportive academic environment and many exciting adventures over the years. Finally, a special thanks to my family for supporting my studies over the years.

This work was supported by the Atmospheric Science Division of the National Science Foundation under the grant ATM0649570.

CHAPTER 1

INTRODUCTION

The Arctic has been warming rapidly over the last century, accompanied by a longer melt season, significant sea ice decline, permafrost loss, glacial retreat, and major ecological shifts (Solomon et al., 2007). General circulation models predict amplified polar warming and an ice free Arctic by the mid 21st century Winton (2006). However, these same models underestimate the observed warming and dramatic ice loss over the past decades (Kato et al., 2006; Shindell and Faluvegi, 2009), suggesting they may also underestimate future warming. Much of the uncertainty in Arctic climate prediction originates from the lack of understanding of feedback processes between clouds and sea ice occurring as the Arctic is warming (Vavrus, 2004). Also, the Arctic is particularly sensitive to many short-lived pollutants with various warming and cooling effects that are not well quantified and furthermore, future emissions for these pollutants are subject to possible dramatic changes (Quinn et al., 2008).

Pollution aerosols are of particular interest because on the global scale, observations and modeling studies suggest that their effects on cloud albedo may be sufficient to offset a considerable portion of the warming effects of anthropogenic greenhouse gas emissions (Nakajima et al., 2001; Sekiguchi et al., 2003; Lohmann and Feichter, 2005; Myhre et al., 2007; Solomon et al., 2007). In addition to greenhouse gases, combustion of fossil fuels and biomass releases small aerosol particles that interact with clouds making them visually brighter and more reflective to incoming solar radiation. Although aerosols are relatively short lived in the atmosphere, emissions are large enough that anthropogenic aerosols are

found to be globally distributed, even impacting clouds in remote regions like the Arctic.

The Arctic was long thought to be clean and unpolluted due to the extreme remoteness of the region. However, since the early 1950s a thick haze of aerosols and gaseous pollutants has been observed throughout the Arctic basin seasonally every winter and spring (Barrie, 1986). This "Arctic haze" is now understood to be the result of unique wintertime meteorological conditions allowing pollution transported from mid-latitudes to accumulate until the late spring (Stohl, 2006). Pollution removal is inhibited because a persistent wintertime surface temperature inversion limits vertical mixing and turbulent aerosol deposition. Meanwhile, the cold and dry Arctic atmosphere results in minimal wet scavenging (Law and Stohl, 2007). The Arctic haze rapidly dissipates in the spring, primarily due to the increased efficiency of wet scavenging in the warmer weather (Garrett et al., 2010). Reduced transport efficiency from mid-latitudes also plays a role.

Studies of clouds forming in this pronounced haze have found that aerosol induced changes in cloud thermal emission create a significant surface warming effect (Garrett et al., 2004; Lubin and Vogelmann, 2006; Mauritsen et al., 2010) while changes in cloud albedo leads to cooling during the summer months over the open ocean and snow free surfaces (Lubin and Vogelmann, 2007). A comprehensive basin wide evaluation of the effects of pollution aerosols on Arctic clouds has not been performed. Yet in the Arctic, aerosol indirect effects are estimated to have the largest positive anthropogenic radiative forcing after CO_2 (Quinn et al., 2007). Here, this thesis presents a regional space-based evaluation of the indirect effects of pollution on Arctic cloud properties during the transition from a highly polluted winter to a relatively clean summer. Factors influencing the sensitivity of Arctic cloud properties to pollution are evaluated and should help facilitate an improved estimate of the regional radiative impact of aerosol indirect effects. The following two sections describe in more detail the effects of aerosol pollution on clouds and strategies for using satellites to study the aerosol indirect effect in the Arctic.

1.1 Prior Studies of Aerosol Indirect Effects

Cloud formation relies on the availability of both condensable water vapor and sufficient concentrations of hygroscopic, submicron, aerosol particles acting as nucleation points for cloud droplet formation, called Cloud Condensation Nuclei (CCN). Although, observed CCN concentrations can vary dramatic for any given location, continental regions typically have the highest concentrations of CCN, often in thousands cm^{-3}, while oceanic CCN usually number in hundreds cm^{-3} and remote regions in the Arctic concentrations of CCN less than 1 cm^{-3} have been observed (Bigg et al., 1996; Bigg and Leck, 2001). Concurrent with these differences in CCN, continental clouds typically have smaller and more numerous cloud droplets than similar clouds forming over oceanic and Arctic regions.

Enhanced concentrations of CCN allow for a greater number of cloud droplets to activate during cloud formation. If the total liquid water in the cloud stays constant, this results in more numerous smaller droplets relative to cleaner conditions (Twomey, 1977; King et al., 1993; Hobbs et al., 2000). As a consequence, the cloud optical depth and albedo increase, which, over oceans and dark surfaces the brighter clouds can create a substantial cooling effect (Twomey, 1977). Although significant on a global scale (Lohmann and Feichter, 2005), the indirect effect surface cooling is thought to be small in the Arctic due to low pollution levels during the summer and a generally highly reflective surface (Garrett et al., 2002). A more significant aerosol indirect effect in the Arctic involves changes in cloud thermal emission. When CCN levels are enhanced during polluted conditions, thin low level clouds have increased thermal emissivity, adding an additional flux of thermal longwave radiation to the surface, leading to a significant warming effect (Lubin and Vogelmann, 2006; Garrett and Zhao, 2006; Mauritsen et al., 2010). Furthermore, compared to lower latitude regions, CCN concentrations are often orders of magnitude lower in the Arctic (Bigg and Leck, 2001; Wylie and Hudson, 2002), often making cloud formation limited by the availability of CCN. As a consequence, Arctic clouds may be exhibit increased sensitivity to perturbations in aerosol concentrations due to the relative scarcity of CCN

leading to higher values of IE (Garrett et al., 2002; Garrett et al., 2004; Lihavainen et al., 2009).

Ship-tracks are narrow bright lines forming in marine stratiform cloud decks caused by the emissions from low grade fossil fuel combustion from large shipping vessels (Figure 1.1). Studies of ship-track clouds provided the first direct evidence that shallow unpolluted clouds can be modified in a dramatic way by the addition of a strong but highly localized source of anthropogenic pollution.

Direct observations have found that ship-track clouds are characterized by increased droplet number concentrations, smaller droplet radii and a higher albedo (King et al., 1993;

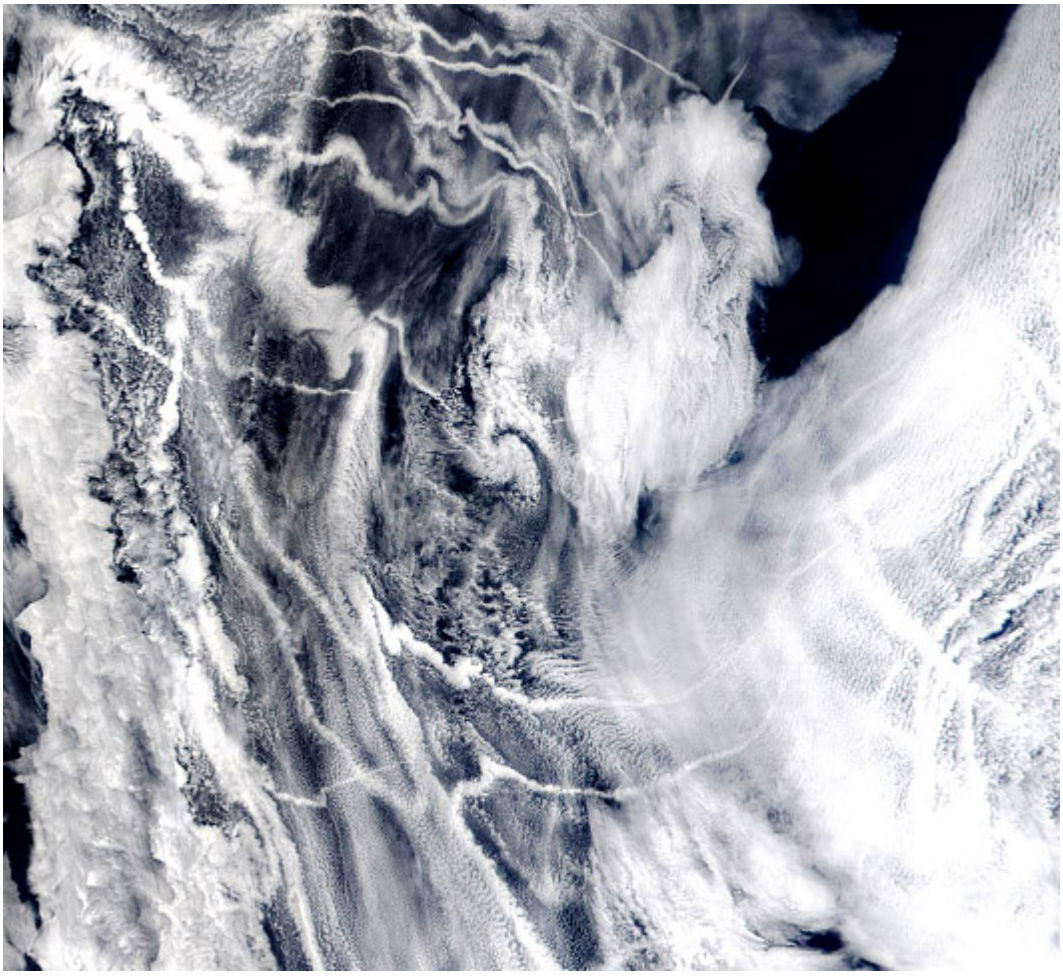

Figure 1.1: A classic example of the first and second aerosol indirect effects viewed from space. Image from taken from http://rapidfire.sci.gsfc.nasa.gov/.

Ferek et al., 1998; Hobbs et al., 2000). Additionally, cases of elevated liquid water content (LWC) and suppressed precipitation compared to adjacent unpolluted clouds have also been observed (Radke et al., 1989; Ferek et al., 2000), suggesting aerosols also affect cloud macro-physical properties, such as cloud lifetime and cloud cover, through perturbations to precipitation processes.

Modeling studies and observations have found evidence that smaller cloud droplet sizes associated with the aerosol indirect effect can suppress collision coalescence processes responsible for warm rain initiation. This reduces the dominant sink of condensate in liquid phase clouds potentially increasing the cloud water content and lengthening the lifetime of the cloud (Albrecht, 1989; Radke et al., 1989; Ferek et al., 2000; Han et al., 2002). However, further studies have shown that due to a myriad of dynamical considerations, there is no simple association between aerosol concentrations, precipitation and cloud liquid water content (Durkee et al., 2000; Ackerman et al., 2004; Lu and Seinfeld, 2005). For example, Xue and Feingold (2006) used computer model simulations to find that, although elevated aerosol concentrations tend to suppress precipitation processes, there is also an overall reduction in cloudiness due to stronger evaporation of the smaller cloud droplets and an increase in the entrainment of dry air.

The overall climatic impact of how secondary aerosol indirect effects relate to precipitation and cloud lifetime is largely inconclusive. This is because the processes and potential feedbacks involved are highly complex and difficult to observe in the climate system (Ackerman et al., 1993; Han et al., 2002; Stevens and Feingold, 2009). Recent advances in satellite remote sensing, with near global coverage and now relatively long-term datasets, are allowing a much better understanding of the impacts of aerosol-cloud interactions on a global scale (Lohmann and Feichter, 2005).

1.2 Study of Aerosol-Cloud Interactions from Space

For more than a decade, a variety of advanced satellite instruments, such as the AVHRR (Advanced Very High Resolution Radiometer), MODIS (Moderate Resolution Imaging Spectroradiometer) and POLDER (Polarization and Directionality of the Earth's Reflectance), have been providing high resolution cloud property and aerosol data that have allowing many studies to adopt a space-based approach to investigate aerosol-cloud interactions on regional and global scales (Nakajima et al., 2001; Bréon et al., 2002; Kaufman et al., 2005; Myhre et al., 2007). More recently, with the successful launch of the A-train and some of its specialized satellites, for example CALIPSO, for the first time the vertical structure and distribution of aerosols and clouds can be viewed from space. Satellites are highly useful for studying aerosol-cloud interactions because, for one, they directly observe actual clouds at near global coverage. Additionally, the aerosol indirect effect is thought to have a large climatic forcing (Solomon et al., 2007). Because satellites observe aerosols and clouds over a long period of time on a global level, they can provide reasonable estimates of climate forcing related to the aerosol indirect effect (Lohmann and Feichter, 2005).

Space borne measurements make it possible to study cloud optical properties with the coincident presence of aerosols. However cloud and aerosol information cannot be retrieved simultaneously from the same satellite instrument. In order to assess aerosol-cloud interactions, a commonly employed strategy pairs aerosol retrievals with clouds in adjacent airmasses. The assumption is then made that aerosol concentrations are horizontally homogeneous (Feingold et al., 2001; Sekiguchi et al., 2003). Using this approach allows a statistical correlation to be made between regional aerosol concentrations and cloud properties. However, it is difficult to determine whether there is an actual physical interaction occurring. For example, aerosol optical depth and cloud fraction can both be correlated with static stability (Mauger and Norris, 2007) and are not actually acting independent to each other. Additionally, the vertical distribution of aerosols is difficult to establish using passive satellite retrievals: if the aerosol are not vertically co-located with clouds then by

definition there cannot be an aerosol indirect effect.

An alternate, less subjective space-based strategy for evaluating the aerosol indirect effect uses pollutant or aerosol fields produced by a chemical tracer transport model that are co-located with satellite retrievals of cloud properties (Schwartz et al., 2002; Kawamoto et al., 2006). For instance, Schwartz et al. (2002) used column sulfate burden as a pollution tracer that was collocated with cloud retrievals from AVHRR. Although superior to entirely satellite based studies, this approach is problematic for two reasons. First, pollution is not necessarily vertically homogeneous. As a consequence, the column burden might not be representative of what is experienced at cloud level. Furthermore, sulfate is not necessarily an independent quantity free from feedback mechanisms that affect the sensitivity of clouds to pollution. During a cloud's lifetime, concentrations of sulphate aerosols may decrease through precipitation or increase through aqueous-phase oxidation. Because sulphate aerosols influence the droplet sizes of clouds, they also alter the rates of cloud processing and precipitation, thus affecting their own concentrations. It is not possible to evaluate the clouds sensitivity to pollution if the independent quantity used (e.g., the sulfate burden) is not in fact independent of the clouds themselves.

The cloud-aerosol feedback difficulties can be avoided by using a truly passive tracer such as carbon monoxide (CO) to represent pollution aerosols. CO is a product of incomplete combustion where near industrial sites perturbations of CO generally correlate well with anthropogenic CCN in a nonprecipitating air-mass (Longley et al., 2005; Garrett et al., 2006). Also, CO emitted by agricultural and large forest fires has been shown to be highly correlated with many aerosol and trace gases found in Arctic pollution plumes sampled by aircraft (Stohl et al., 2007; Warneke et al., 2009; Paris et al., 2009). CO serves an ideal tracer of pollution because the relatively inert gas, insoluble in cloud droplets, that has a lifetime on the order of months, so that, on short time scales, atmospheric concentrations are determined primarily by mixing and dilution. The aerosol indirect effect computed with respect to a passive tracer like CO will act to remove some of the bias related to comparing

satellite derived aerosols and clouds, and the CO and clouds will be independent of each other.

A passive tracer like CO, whether modeled or observed, has shown to be very useful for diagnosing aerosol-cloud interactions (Garrett et al., 2006; Avey et al., 2007; Brioude et al., 2009; Garrett et al., 2010). For example, a recent study by Avey et al. (2007) combined satellite retrieved cloud products with fields of CO concentrations from a tracer transport model in order to characterize the aerosol indirect effect. On account of the high vertical resolution of the tracer transport model, Avey et al. (2007) were able to compare co-located cloud properties with pollution tracer concentrations, finding a large aerosol indirect effect occurring off the east coast of the United States. They were able to ascertain that wet-scavenging of aerosols likely caused the indirect effect to be limited to near the coast because the sensitivity of cloud properties to the passive pollution tracer diminished downwind from the pollution source in the regionally precipitating cloud mass.

Removal of aerosol from pollution plumes is not well understood largely because it is difficult to directly observe. Anthropogenic aerosols and CO share the same source, and they are both affected by the same atmospheric transport processes, but aerosol are also affected by chemical and removal processes. Thus, it is possible to indirectly quantify aerosol removal through the use of a passive tracer like CO (Garrett et al., 2006; Avey et al., 2007).

Here, pollution-cloud interactions in the Arctic are studied by comparing modeled passive pollution tracers to satellite retrieved cloud properties. The use of a passive tracer provides a more comprehensive description of pollution-cloud interactions because it indicates conditions that allow for pollution to have large impact on clouds. Additionally, when the cloud sensitivity to the tracer is minimal, it is possible to ascertain information on physical processes that act to remove cloud active components of pollution. The goal is to be able to describe the aerosol indirect effect with respect to pollution plumes advected into the Arctic and to characterize some of the physical and thermodynamic factors that

influence the sensitivity of clouds to pollution.

1.3 Thesis Objectives

The format of the thesis will proceed in the following manner. Chapter 2 will examine the process of quantitatively evaluating the aerosol indirect effect on observable cloud microphysical properties and how aerosols also influence cloud macro-physical properties. Chapter 3 describes the cloud products that are retrieved using the MODIS and POLDER instruments on A-Train satellites Aqua and Parasol, respectively, and also includes a description of the tracer transport model FLEXPART that provides tracers for anthropogenic and biomass burning emissions.

Chapter 4 describes the approach and methodology used here to quantify, as accurately as possible, pollution-cloud interactions in the Arctic. Initially, this process involves comparing and identifying the most suitable combination of satellite cloud property retrievals for Arctic clouds. Secondly, it ensures that the modeled pollution tracer is reaching the Arctic and is representative of in-situ pollution observations. Lastly, a description is provided of the method for assessing the aerosol indirect effect by co-locating vertically, horizontally, and temporally, fields of cloud property retrievals with fields of the pollution tracer.

Chapter 5 presents the results and observations from the analysis of the co-located cloud property and pollution tracer data. Also, an explanation is provided for why the data was analyzed for different constraints and conditions. Chapter 6 describes possible physical processes affecting the results presented and to discuss further research that could help constrain and isolate the physical mechanism governing cloud sensitivity to pollution.

Chapter 7 is a summary of the approach taken to study pollution cloud interactions, a brief synopsis of observations of aerosol indirect effects and lastly a discussion of future avenues of research.

CHAPTER 2

QUANTIFICATION OF AEROSOL INDIRECT EFFECTS

The first aerosol indirect effect states that increases in CCN concentrations lead to more droplets of a smaller size, assuming the total amount of water in the cloud remains constant. This is easily explained because cloud Liquid Water Content (LWC) is related to droplet effective radius (r_e), and droplet number concentration (N_c) through

$$LWC = \frac{4}{3}\rho_w \pi r_e^3 N_c \tag{2.1}$$

where ρ_w is the bulk density of liquid water. Absent any change in LWC, the relation ship between r_e and N_c is

$$\frac{d\ln r_e}{d\ln N_c} = -\frac{1}{3} \tag{2.2}$$

so that any increase in N_c results in a corresponding one third decrease of r_e. Using a similar relationship, the first aerosol indirect effect is typically quantified using the IE parameter, defined by the relative change in a cloud property, generally cloud optical depth (τ) or cloud droplet effective radius (r_e), with respect to a relative change in some aerosol quantity, often satellite retrieved aerosol optical depth (τ_a) (Feingold et al., 2001; Bréon et al., 2002; Lohmann and Feichter, 2005). If the cloud Liquid Water Path (LWP) is held constant, where $LWP = LWC \times h$ and h is the depth of the cloud, then

$$IE = -\frac{d\ln r_e}{d\ln \tau_a}\bigg|_{LWP} \tag{2.3}$$

The rational is that $N_c \propto CCN$ and that CCN concentrations are proportional to the measured aerosol quantity (e.g., τ_a). In this case, the theoretical maximum value of IE is $\frac{1}{3}$, meaning that any increase in measured aerosol results in an equal increase in cloud droplet formation with no impact on the cloud water content (Feingold, 2003). Since measured aerosol quantities don't necessarily describe the amount of CCN sized particles that activate into cloud droplets, and additional variables also influence cloud formation, observed values of IE are generally smaller by a factor of two or more (Twomey, 1977; Nakajima et al., 2001; Feingold et al., 2003; Sekiguchi et al., 2003; Lohmann and Feichter, 2005).

The benefit of assessing the effects of aerosols on clouds using the IE parameter (e.g., Eq. 2.3) is that by considering relative changes in paramaters rather than absolute changes, calculated values of IE are less affected by measurement errors and can be compared using a variety of datasets and proxies for aerosol.

Here, we use a modified form of the IE parameter where the sensitivities of the cloud properties r_e, τ and LWP are compared to fields of Carbon Monoxide (CO) concentrations produced by the FLEXPART Lagrangian particle dispersion model. The fields of CO (χ_{CO}) act as a passive tracer of recent biomass burning and anthropogenic combustion and will be conditionally associated with high levels of CCN.

The advantage of comparing a passive pollution tracer to cloud fields is that pollution and clouds are not coupled and this permits identification of cause and effect in pollution-cloud interactions. Additionally, the use of a passive tracer like χ_{CO} has the benefit of allowing information to be gathered about wet-scavenging of CCN. If concentrations of χ_{CO} are high but the co-located cloud perturbations low, this may be interpreted as an indication that the cloud active components of the pollution field have been removed through

wet scavenging (Avey et al., 2007).

To explain further, since, cloud optical depth (τ) can be expressed as

$$\tau = \frac{3}{2}\frac{LWP}{\rho_w r_e} \tag{2.4}$$

where ρ_w is the bulk density of liquid water, the derivative of the natural logarithm of τ with respect to the logarithm of the χ_{CO} tracer, is

$$\frac{d\ln\tau}{d\ln\chi_{CO}} = -\frac{d\ln r_e}{d\ln\chi_{CO}} + \frac{d\ln LWP}{d\ln\chi_{CO}} \tag{2.5}$$

Since CCN are the active components of pollution plumes, the sensitivity of cloud optical depth to pollution will be product of two partial derivatives evaluated in the following manner:

$$\frac{d\ln\tau}{d\ln\chi_{CO}} = \frac{d\ln\tau}{d\ln CCN}\, S \tag{2.6}$$

where

$$S = \frac{d\ln CCN}{d\ln\chi_{CO}} \tag{2.7}$$

is a scavenging parameter that ranges from 0 to 1 (Garrett et al., 2006, 2010). When the rate of wet scavenging is high, then S will be small, indicating a small relative change in CCN for a relative change in χ_{CO}. Conversely, S is large when minimal amounts of wet scavenging have impacted the pollution plume and the correlation between CCN and χ_{CO} is high. Thus, by calculating the sensitivity of cloud properties to χ_{CO} rather than more commonly used aerosol quantities (e.g., Feingold et al. (2001); Bréon et al. (2002); Kaufman et al. (2005)), an indication to when wet scavenging is affecting pollution plumes

is provided.

While cloud microphysical properties can be influenced by aerosols, they are more fundamentally determined by the meteorological conditions in which they form (Chang and Coakley, 2007). To first order, the amount of liquid water in an adiabatic cloud depends on the difference in moist and dry lapse rates at a certain temperature and pressure according to the basic thermodynamic relationship;

$$\frac{dLWC}{dz} = \frac{\rho_a(T,P)\,C_p}{L_v}\left(\Gamma_d - \Gamma_s(T,P)\right) \tag{2.8}$$

where, $\rho_a(T,P)$ is the air density, C_p is the heat capacity of air, L_v the latent heat of vaporization, Γ_d the dry adiabatic lapse rate and Γ_s the moist adiabatic lapse rate. At colder temperatures the difference in lapse rates is much smaller and consequently less moisture is available for condensation and release of latent heat. For example, a cloud forming at 900 hPa at a temperature of -15°C will have a value of $dLWC/dz$ of 0.7 g m^{-3} km^{-1}. At the same height but a temperature of 0°C, $dLWC/dz$ has a value of approximately 1.9 g m^{-3} km^{-1}.

Thus, in order to limit a meteorological bias and constrain cloud microphysical sensitivity to pollution, we evaluate the sensitivity of cloud properties to χ_{CO} within small bins of temperature and pressure. This minimizes covariance associated with χ_{CO} acting as a tracer of warmer, moister, airmasses that may be influencing the observed cloud properties more than pollution itself.

Furthermore, we examine only low-level, liquid clouds in the Arctic in order to simplify interpretation of the physics and to ease comparison with prior studies that have examined the sensitivity of clouds to pollution aerosols (Garrett et al., 2004; Garrett and Zhao, 2006; Lubin and Vogelmann, 2006; Mauritsen et al., 2010). The effect of aerosols on mixed-phase Arctic clouds is a more complex issue (Curry et al., 1996; Girard et al., 2005; Morrison and Pinto, 2005; Morrison et al., 2008; de Boer et al., 2009) and not directly addressed in this

study.

Here, we calculate the values of IE_{re}, IE_{τ}, and IE_{LWP}, by fitting a linear least squares regression of the natural logarithm of the cloud properties against the natural logarithm of the combined anthropogenic and biomass burning tracers, for a given pressure level and temperature. Thus

$$IE_{re} = -\left.\frac{d\ln r_e}{d\ln \chi_{\text{CO}}}\right|_{T,P} \tag{2.9}$$

$$IE_{\tau} = \left.\frac{d\ln \tau}{d\ln \chi_{CO}}\right|_{T,P} \tag{2.10}$$

$$IE_{LWP} = \left.\frac{d\ln LWP}{d\ln \chi_{CO}}\right|_{T,P} \tag{2.11}$$

CHAPTER 3

MEASUREMENTS

In order to characterize pollution-cloud interactions, we use a combination of satellite retrieved cloud products and a modeled pollution tracer. The cloud products are retrieved using the MODIS, POLDER, and CALIOP instruments on A-train satellites, Aqua, PARASOL and CALIPSO, respectively. The Lagrangian tracer transport model FLEXPART provides a tracer for anthropogenic emissions along with a tracer of biomass burning. The datasets used in this study to examine aerosol-cloud interactions in the Arctic are summarized in Table 1.

3.1 Satellite Retrieved Cloud Properties

The A-train constellation is a unique formation of five polar orbiting satellites flying in proximity to each other since June 2006 (Stephens and et, 2002). The group of satellites offers a diverse suite of passive and active instrumentation that, due to their near simultaneous data acquisition, can be used in a highly synergistic fashion. Here, data from passive and active instruments on the Aqua, PARASOL, and CALIPSO satellites are used to retrieve

Table 1: Cloud products and pollution tracer used in the study

Data Source	Parameter	reference
MODIS-Aqua	Cloud top temp., T_C	
	Cloud Opt. Depth, τ	
	Droplet eff. rad. r_e	King et al. (2005)
POLDER-PARASOL	Cloud top Press. P_{O_2}	Fougnie et al. (2007)
CALIOP-CALIPSO	534 nm attenuated backscatter	Winker et al. (2009)
MODIS-POLDER	Cloud phase index, ϕ	Riedi et al. (2007)
FLEXPART	Pollution tracer, χ_{CO}	Stohl et al. (2005, 2007)

Arctic cloud properties (Figure 3.1).

3.1.1 MODIS-Aqua

The MODIS (Moderate Resolution Imaging Spectroradiometer) aboard the Aqua satellite acquires data in 36 spectral bands, with a spatial resolution of 250 m (0.65 and 0.86 μm), 500 m (0.47, 0.56, 1.24, 1.63 and 2.13 μm), and 1000 m (29 wavelengths ranging from the visible to infrared). MODIS Collection 5 Level-2 retrievals are used to provide cloud-top effective radius (r_e), temperature (T_{CT}) and optical depth (τ) (Platnick et al., 2003; King et al., 2005).

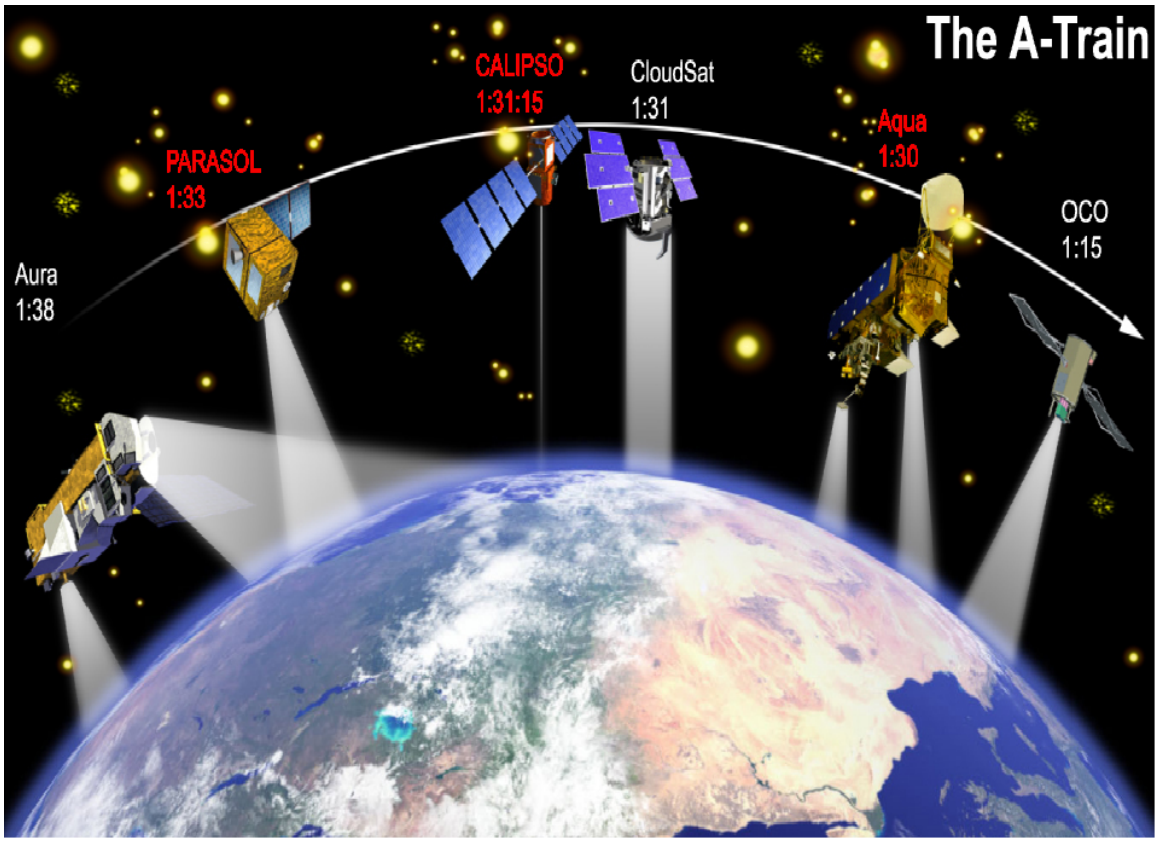

Figure 3.1: A-Train satellite constellation where data from the satellites PARASOL, CALIPSO and Aqua are used in this thesis. (OCO, due to technical difficulties, never joined the A-train group.)

Cloud-top temperatures are determined using the infrared window 11 μm band temperature at 5 km spatial resolution. The retrieval of r_e is made using simultaneous measurements of cloud reflectance from the water absorbing bands (1.6, 2.1, 3.7 μm) combined with one of the non- (or less) absorbing bands (0.65, 0.86, 1.2 μm) depending on the surface conditions. MODIS airborne simulator r_e values in stratiform cloud agree well with in situ measurements of liquid clouds in the Arctic (Platnick et al., 2003). Cloud Liquid Water Path (LWP) is acquired from the MODIS retrieved r_e and τ parameters using the following relationship, where ρ_w is the density of liquid water:

$$LWP = \frac{2}{3} r_e \tau \rho_w \tag{3.1}$$

3.1.2 POLDER-PARASOL

Flying just two minutes behind Aqua in the A-train constellation is the French built micro-satellite PARASOL (Polarization & Anisotropy of Reflectances for Atmospheric Sciences coupled with Observations from a Lidar) carrying a passive radiometer/polarimeter called POLDER (Polarization and Directionality of the Earth's Reflectance) that provides systematic measurements of spectral, directional and polarized characteristics of reflected sunlight (Fougnie et al., 2007). This unique multidirectional instrument provides cloud microphysical parameters at a spatial resolution close to 20 km $\times$ 20 km.

Here, cloud pressure is determined from the POLDER cloud oxygen pressure (P_{O_2}), which is based on the differential absorption measured at 763 and 765 nm wavelength, corresponding to the A-band region of strong absorption by atmospheric oxygen (Bréon and Colzy, 1999). Multiple scattering in cloud places P_{O_2} values more towards the center of the cloud rather than cloud top. Nonetheless, P_{O_2} cloud top pressure from POLDER is preferred over MODIS cloud top pressure retrievals because the P_{O_2} algorithm does not utilize infrared channels that require an assumed temperature profile (Buriez et al., 1997; Weisz et al., 2007). Thus, it is unaffected by the presence of surface temperature inversions,

which can be common in the Arctic (Shupe et al., 2006). The selection of this particular cloud height retrieval is described in section 4.

3.1.3 Cloud Phase

One of POLDER's unique capabilities is being able to measure the polarization of radiation reflected off clouds from a range of different angles. When clouds are composed of liquid spherical particles there is a strong maximum in the polarized component of the reflected radiation at about 140° while the polarization of the radiation drops to zero for radiation reflected at an angle of 90° (Figure 3.2). These features make possible the discrimination of liquid clouds from those composed of ice particles, which do not exhibit these same polarization features. Unambiguous discrimination between ice particles and liquid water droplets can be made using these polarization differences (Goloub et al., 2000) and the results can be easily be viewed visually in the form of the phenomenon referred to as "cloud bow" (Figure 3.3).

Alternatively, MODIS makes use of the strong differences in the spectral absorption characteristics of ice and water in the 8.5 μm and 11 μm radiation bands for one phase retrieval (Platnick et al., 2003). The MODIS phase will be a 'radiative' rather than physical phase meaning that in a mixed phase cloud with uneven distribution of ice crystals to liquid water droplets, the dominant phased particles will often determine the radiative phase of the cloud. For example, a cloud with a few large ice crystals and more numerous smaller droplets will be classified as liquid phase due to the droplets dominating the radiative signature. Unfortunately, at temperatures below 273 K the phase becomes more ambiguous as the difference in emission characteristics of supercooled water droplets and ice crystals becomes small. Additionally, water vapor in the atmosphere and surface emissivity can be highly variable and can influence the radiative signature that the retrieval relies on and results in errors and biases, although primarily affecting low-level cloud.

An additional MODIS phase retrieval uses measurements of shortwave infrared re-

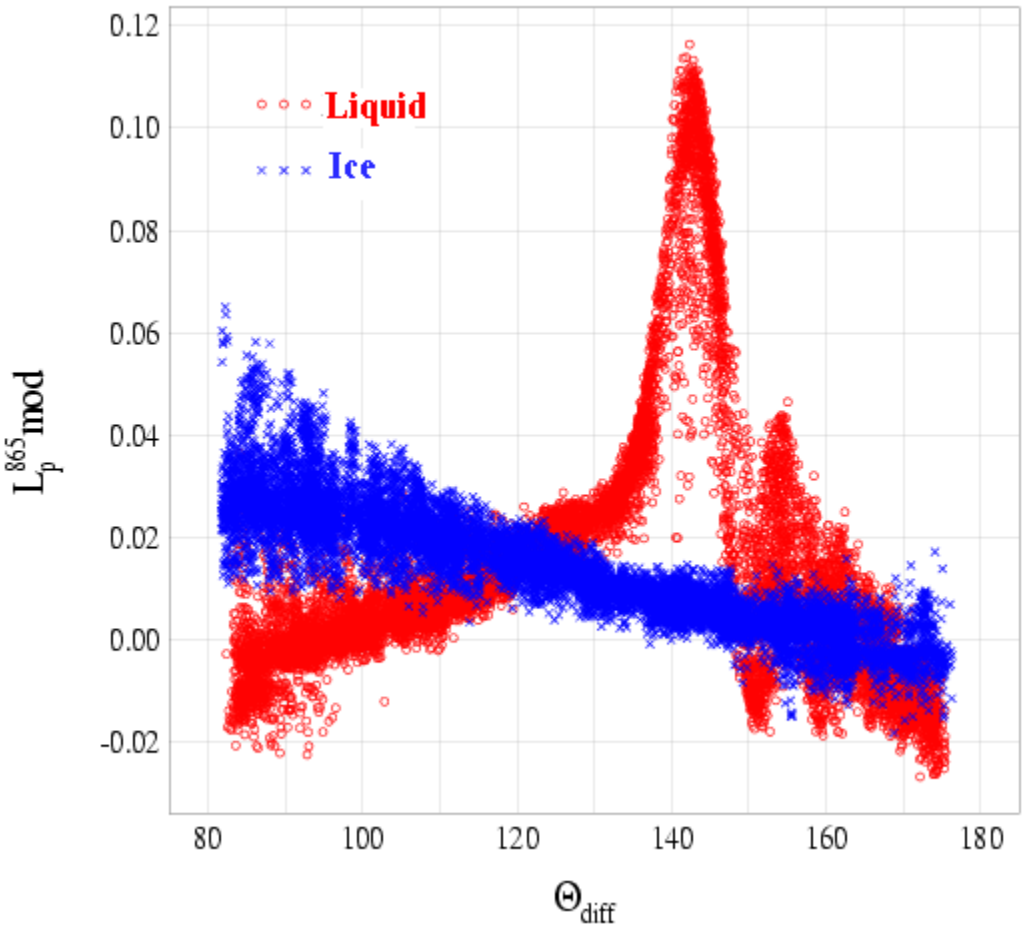

Figure 3.2: Polarization of reflected radiation is plotted as a function of scattering angle for cloud ice crystals and cloud droplets. For liquid cloud droplet a pronounced peak in polarized reflectance occurs at the scattering angle of 140° . Image is courtesy of Jérôme Riedi, Université Lille, France.

flectance (SWIR) at the wavelengths 1.6 and 2.1 μm and visible reflectance in the visible channels (King et al., 2003). Essentially, the retrieval takes advantage of that fact that ice particles absorbing slightly more radiation at SWIR wavelengths than liquid water droplets while the visible reflectance will be effectively equal. The phase retrieval becomes ambiguous when the ice crystals are relatively small, the liquid droplets are large or when the clouds are relatively thin. One advantage to this retrieval is that it is not subject to a temperature bias or surface emissivity properties.

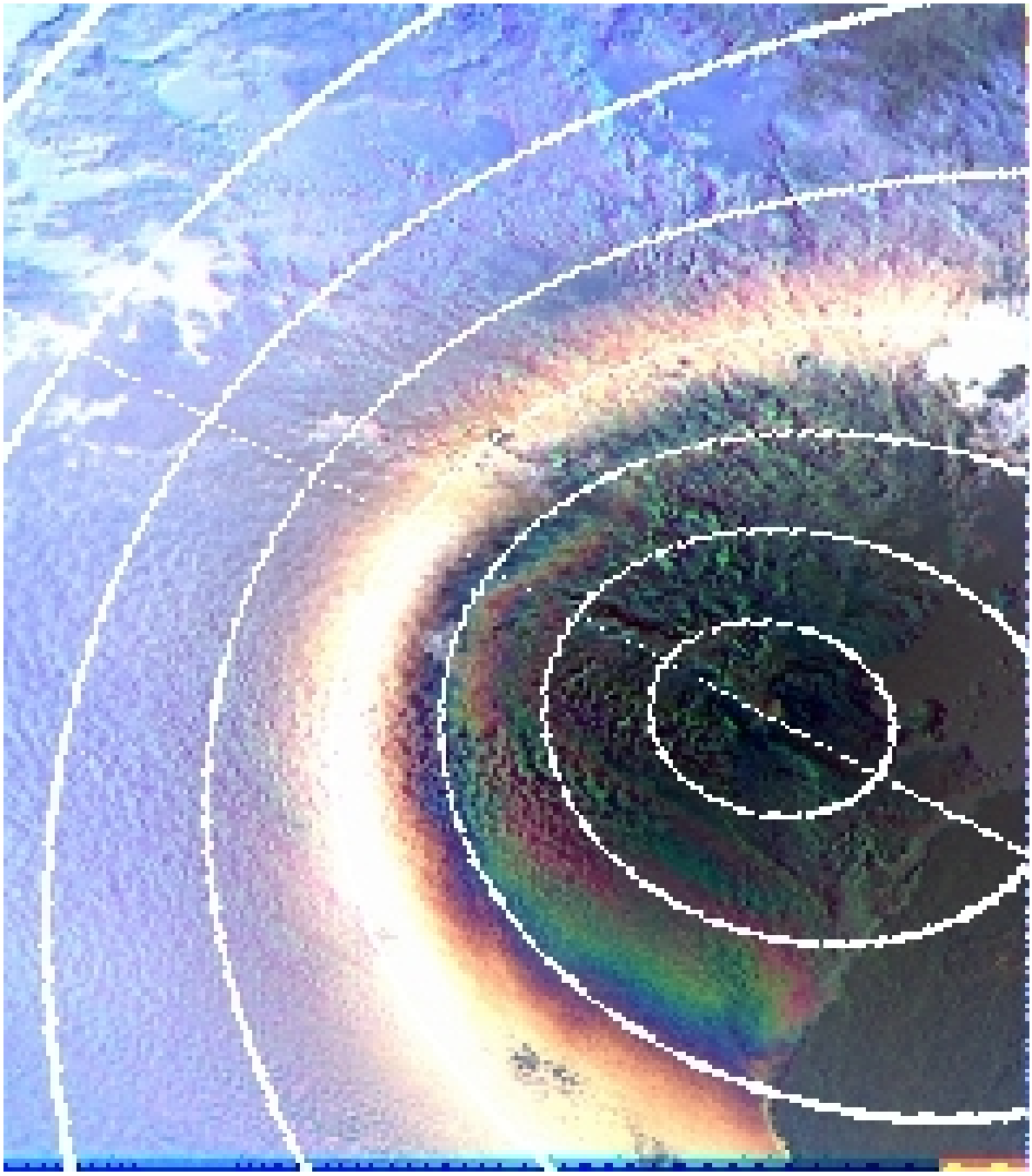

Figure 3.3: Shown here is a specific example image of polarized reflectance data from a liquid phase cloud retrieved by the POLDER instrument demonstrating the prominent "cloud bow" associated with the peak in polarized reflectance occurring at the scattering angle of 140° .

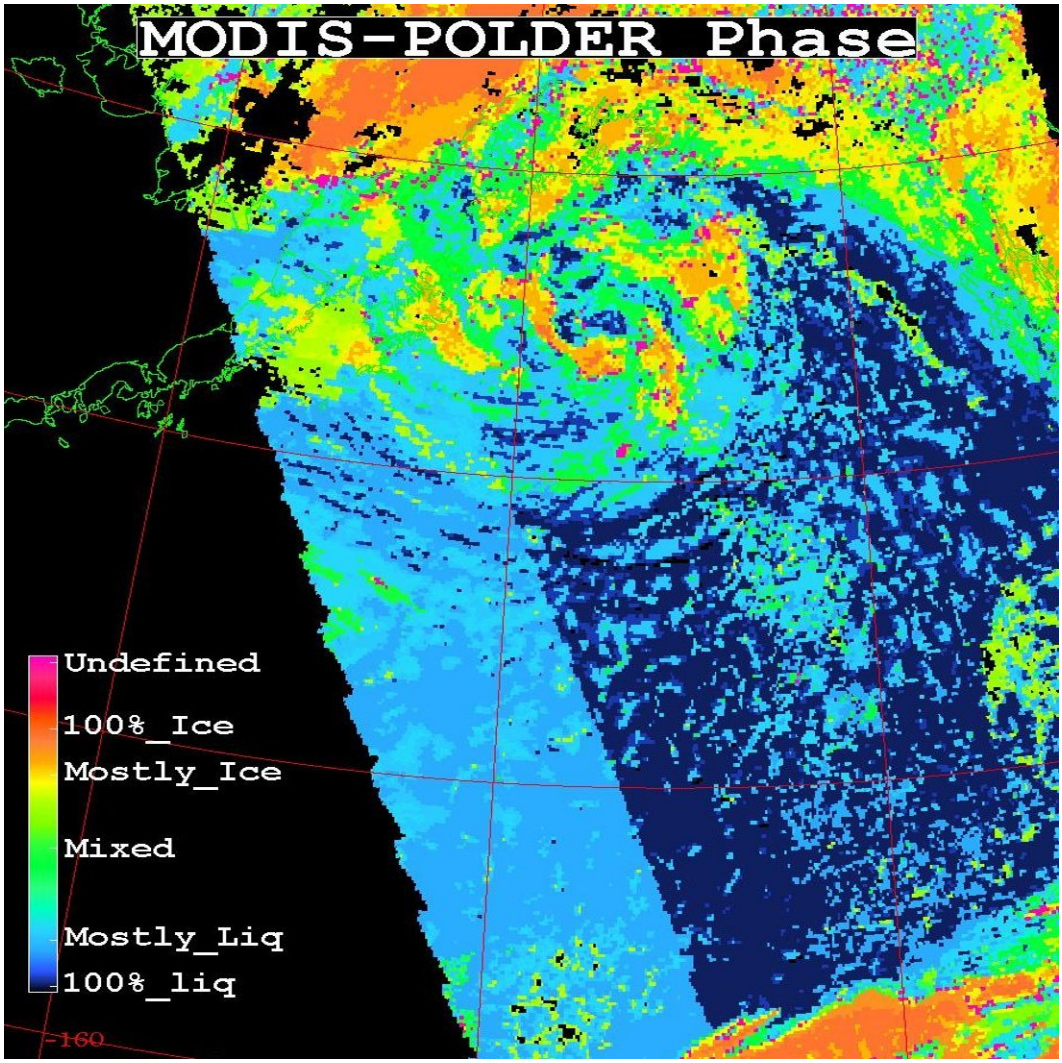

Figure 3.4: Cloud phase determined from merged MODIS and POLDER data retrievals based on a confidence index ranging from Confident liquid (1) to Confident ice (200). The sampling footprint is smaller for the POLDER instrument and when the phase data are included in the algorithm, the confidence in the phase determination improves significantly.

While each of the three phase retrievals has its own set of advantages and limitations, the configuration of the A-train satellite group allows for the retrievals to be used in a synergistic combination resulting in an overall improvement of cloud phase determination. Here, cloud phase is determined by a novel algorithm developed by Riedi et al. (2007), that combines the previously mentioned POLDER and MODIS phase retrievals to provide a semicontinuous confidence index (ϕ) for thermodynamic phase, ranging from confident liquid (1) to confident ice (200) .

Figure 3.4 shows an example of the merged phase retrieval for a low-level cloud deck forming near southern Alaska. POLDER has a slightly smaller footprint which demonstrates how when the MODIS and POLDER products are combined the overall confidence improves. The rationale for merging the three methods is for multiple reasons. First, any single phase retrieval method may be unable to provide a definitive cloud answer while one of the other two may be able to. When multiple retrievals are in a agreement, a higher level of confidence in the phase is provided. Additionally, when the phase retrievals are in disagreement indicates situations with potential multiple layered clouds, mixed-phase clouds or heavy aerosol loadings.

Here, the analysis of is constrained to Arctic clouds found to have a value of ϕ that is 50 or below, that are assumed to be liquid because it requires that at least two of the three retrieval algorithms used in the index agree on phase determination. Although we use this liquid phase constraint, the possibility of ice precipitation is not excluded. A common but tenuous regime of supercooled liquid clouds precipitating ice, is frequently observed in the Arctic (Curry et al., 1996; Intrieri et al., 2002). Due to the nature and limitations of passive satellite remote sensing, cloud property retrievals are most sensitive to conditions at cloud top and little information is usually available below the upper 100 m of the cloud.

3.1.4 CALIOP

The A-train satellite group contains two active remote sensing instruments, CloudSat's 94-GHz cloud profiling radar Stephens and et (2002) and CALIPSO (Cloud-Aerosol Lidar and Infrared Pathfinder Satellite Observation)'s 532-nm and 1064-nm Cloud- Aerosol Lidar with Orthogonal Polarization (CALIOP) lidar which for the first time allow a detailed vertical structure of Arctic clouds to be viewed from space. CALIOP utilizes three receiver channels: one measuring the 1064-nm backscatter intensity and two channels measuring orthogonally polarized components of the 532-nm backscattered signal. While both instruments provide a much more accurate cloud height retrieval over passive instruments,

CloudSat is incapable of identifying clouds in the lower km of the atmosphere due radar backscatter and surface clutter. Although CALIOP suffers from the same low level retrieval problems, because of its shorter lidar pulse length it can identify clouds down to 500 m above the surface (Winker et al., 2009) and is used preferentially over CloudSat.

Prior studies have shown biases exist between cloud top heights derived from the MODIS, POLDER and CALIOP instruments (Weisz et al., 2007; He et al., 2009; Yao et al., 2010), with CALIOP most closely representing the actual physical location of the cloud. The biases are highly variable and dependent on the specific cloud being measured and its location in the atmosphere. Since the literature does not specifically describe a bias for low-level Arctic clouds, here, CALIOP 532 nm total backscatter product is used to identify cloud top heights that are used as a benchmark to compare passive cloud top height products from the MODIS and POLDER.

3.2 Anthropogenic and Biomass Burning Pollution Tracer

The Lagrangian particle dispersion model FLEXPART (Stohl et al., 2005) is used here to characterize the transport of pollution into the Arctic. The model is driven by the European Centre for Medium Range Weather Forecasts (ECMWF) re-analyses (0000, 0600, 1200, 1800 UTC) and forecast (0300, 0900, 1500, 2100 UTC) products (EMCWF, 2002) and produces pollution tracer output at 15 tropospheric vertical model levels, with a global horizontal resolution of 0.5° x 0.5° in 3-hour time steps. Superimposed onto the meteorological products, is a parametrization of turbulence in the atmospheric boundary layer and free troposphere, based on solutions to Langevin equations (Stohl and Thomson, 1999). FLEXPART calculates the trajectories of tracer particles using the mean winds interpolated from the meteorological analysis fields plus the random motions representing turbulence and an additional parametrization to describe moist convective transport (Forster et al., 2007). North of 75°, FLEXPART advects particles using a polar stereographic projection in order to maintain a high degree of accuracy at these extreme latitudes.

Anthropogenic emission sources are calculated from the EDGAR emission inventory (Olivier and Berdowski, 2001). The general distribution of Northern Hemisphere anthropogenic pollution sources is shown in Figure 3.5, a plot of the annual mean emission rates of Carbon Monoxide (ng m^{-2} s^{-1}). The dotted black line represents the position of the mean wintertime (Dec - Mar) "Arctic Front", defined by the largest gradient in potential temperature (Law and Stohl, 2007) that serves as a direct barrier to isentropic pollution transport. Northern Europe is the only region with significant emission sources inside the Arctic front. In addition to anthropogenic pollution, a tracer of biomass burning is incorporated into the model based on a fire detection scheme from the MODIS instruments on Aqua and Terra (Giglio et al., 2003) using an algorithm described by Stohl et al. (2007).

Initially validated using regional scale tracer studies (Stohl et al., 1998), the FLEXPART model has now been used extensively in Arctic pollution related studies, often concurrent with field campaigns corroborating the accuracy of the model (Stohl et al., 2006; Warneke et al., 2009; Paris et al., 2009; Hirdman et al., 2010). For example, during the IPY airborne field experiments, ARCTAS (Arctic Research of the Composition of the Troposphere from Aircraft and Satellites) and ARCPAC (Aerosol, Radiation, and Cloud Processes affecting Arctic Climate), FLEXPART was used to predict locations of pollution plumes in order to select appropriate flight plans for in situ pollution measurements (Fuelberg et al., 2010; Jacob et al., 2010). Not only were pollution plume locations accurate, predicted CO enhancements agreed well with the airborne measurements (Warneke et al., 2010).

Close to emission sources, anthropogenic CO generally correlates well with anthropogenic CCN in a nonprecipitating air-mass (Longley et al., 2005). In the Arctic, when precipitation is low, short-term CO perturbations (most likely anthropogenic in origin) are associated with strong values of aerosol light scattering, which is a proxy for CCN sized aerosols (Garrett et al., 2010). Unlike CCN, however, the χ_{CO} tracer does not interact with or influence clouds and will be conditionally related to aerosol concentrations. The passive

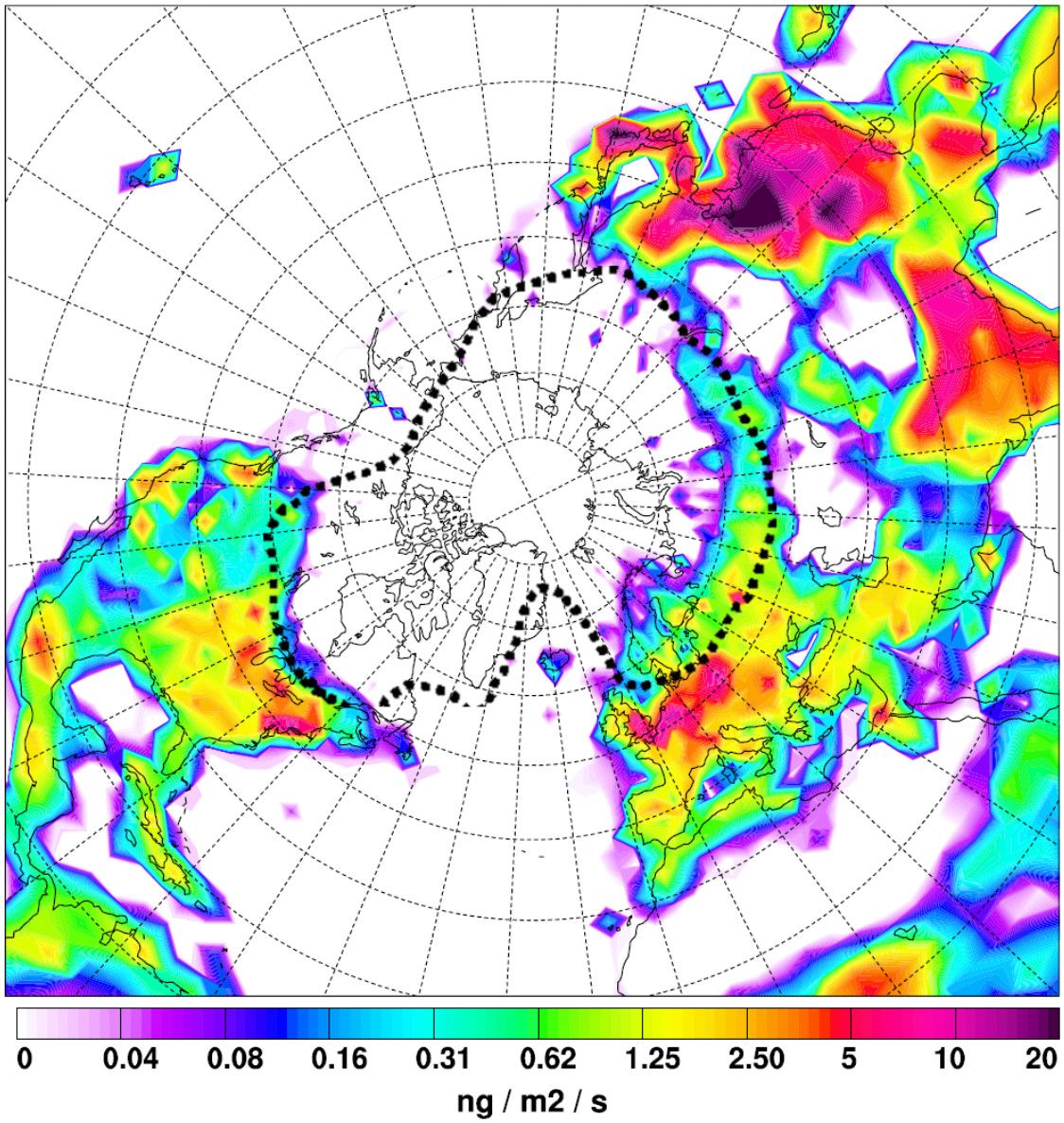

Figure 3.5: Annual mean emission rates of Carbon Monoxide (ng m^{-2} s^{-1}), used as tracer of anthropogenic and biomass burning combustion that is ingested into FLEXPART tracer transport model and followed for 20 days, courtesy of Andreas Stohl and accessed from: http://zardoz.n ilu.no/~andreas/flextra+flexpart.html. Dotted line represents the mean position of the wintertime (Dec - Mar) "Arctic Front" based on NCEP reanalysis data.

nature of the χ_{CO} tracer from FLEXPART means that it is affected only by dilution up to a point of instantaneous removal at twenty days atmospheric residence time. The advantage of comparing a passive pollution tracer to cloud fields is that pollution and clouds are not coupled and this permits identification of cause and effect in pollution-cloud interactions.

For the Spring and Summer of 2008 IPY studies, pollution and biomass burning (BB) tracer data were simulated for the period March 21 through July 20 with tracer output in 3 hour increments representing the average concentration of that grid cell over the previous three hours.

CHAPTER 4

METHODS

4.1 FLEXPART Verification

Prior to analyzing cloud properties with the FLEXPART pollution tracer, I performed two assessments of the validity and accuracy of FLEXPART as a proxy for pollution aerosols. This also served to test the co-location method using different datasets. First, I compared modeled χ_{CO} concentrations to in situ CO measurements from the Barrow, Alaska Department of Defense ARM (Atmosphere Radiation Measurement) site. Second, I co-located FLEXPART total column concentrations with MODIS aerosol optical depth retrievals.

The χ_{CO} and sampled in-situ CO cannot be meaningfully compared directly because the in situ measurements are total CO concentrations sampled hourly by a flask, while χ_{CO} is only representative of a short-term perturbation above some background value of CO. The lifetime of CO in the Arctic varies from weeks to months depending on the season because its primary sink is through the photolytic reaction with the hydroxyl radical. The absence of sunlight in the wintertime leads to pronounced seasonal cycle in CO concentrations. The sampled flask CO concentrations are a combination of CO from recent pollution events along with a time dependent background of CO concentrations, whereas χ_{CO} is representative of pollution events occurring in the previous 20 days.

Figure 4.1 shows in situ CO data sampled every hour, flask measurements obtained approximately weekly ("event"), and monthly-averaged CO data Barrow, Alaska. Based on Figure 4.1 and previous values estimated in the literature (Garrett et al., 2006; Paris et al.,

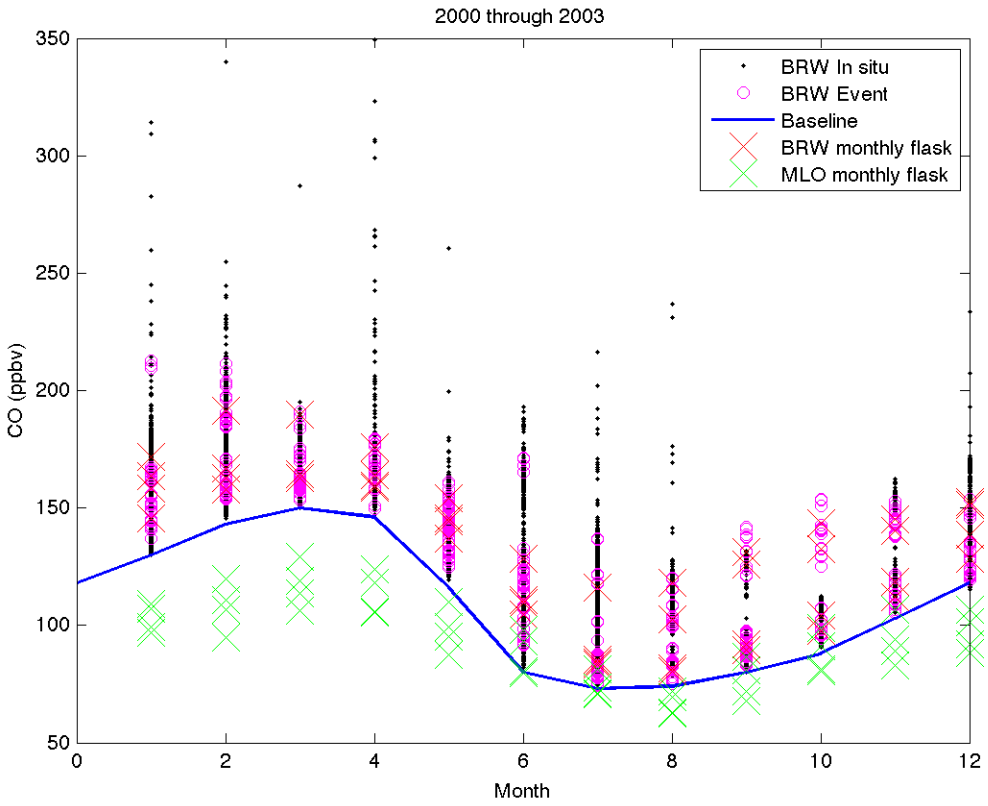

Figure 4.1: In situ flask data sampled every hour ("in situ"), approximately weekly ("event"), and monthly averaged CO data from Barrow, Alaska. Data from CMDL: http://www.esrl.noaa.gov/gmd/BRW. A lower latitude unpolluted reference site from Mauna Loa (MLO) is also plotted.

2009; Warneke et al., 2010), I assume that the background value of CO concentrations at Barrow has a nonlinear decrease from 150 ppb starting March 20 to 90 ppb at the end of the comparison on July 21. Subtracting out this background value of CO concentrations from the hourly in-situ CMDL data for 2008 allows a comparison of χ_{CO} to in situ ΔCO values, Figure 4.2.

Figure 4.2 shows that FLEXPART χ_{CO} rather effectively modeled the variability in ΔCO values from in situ measurements. This is an encouraging observation because, not only does χ_{CO} emitted from warmer lower latitude regions have to travel a large horizontal distance to reach Barrow Alaska, but the χ_{CO} tracer would also have to be vertically mixed downward in order for it to be present in the grid cell located above Barrow Alaska. This is

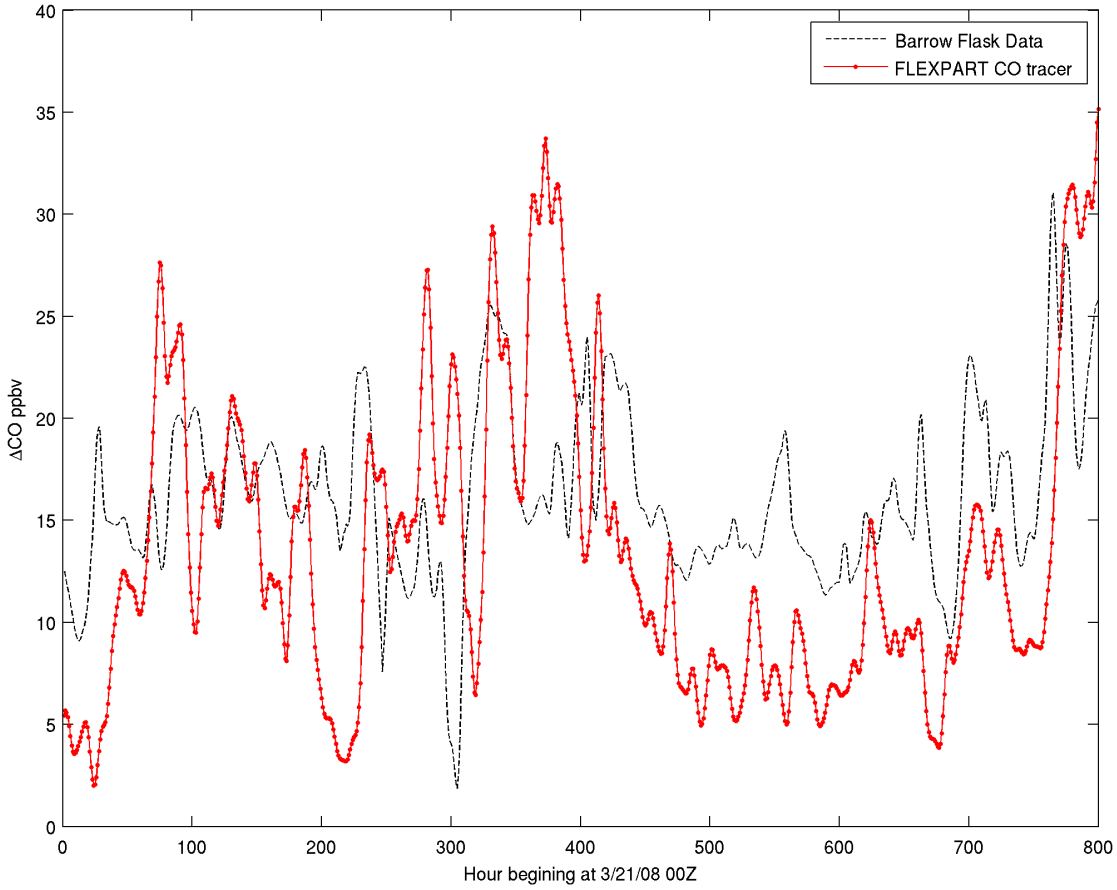

Figure 4.2: Time series of FLEXPART χ_{CO} concentrations for the 0 to 200m layer for the gridbox overlaying Barrow Alaska at 71 ° North and 156.5° West, plotted with the time series for the Barrow ARM site hourly flask ΔCO measurements (Background CO value is removed).

a positive sign that the parametrized turbulence used by FLEXPART (Stohl and Thomson, 1999) is realistically transporting tracer particles across vertical atmospheric layers. This exercise also indicates that during this time period a large portion of the ΔCO variability at Barrow can be explained by long range pollution transport and not localized sources.

MODIS provides aerosol retrievals for cloud free conditions. The focus of this study is on analyzing the effects of co-located aerosol and clouds, however, useful information about relative aerosol amounts can be gained by comparing FLEXPART to MODIS aerosol retrievals. Also, it helps demonstrate the validity of using FLEXPART tracers to study the aerosol indirect effect and it allows a visual confirmation that the co-location procedure is

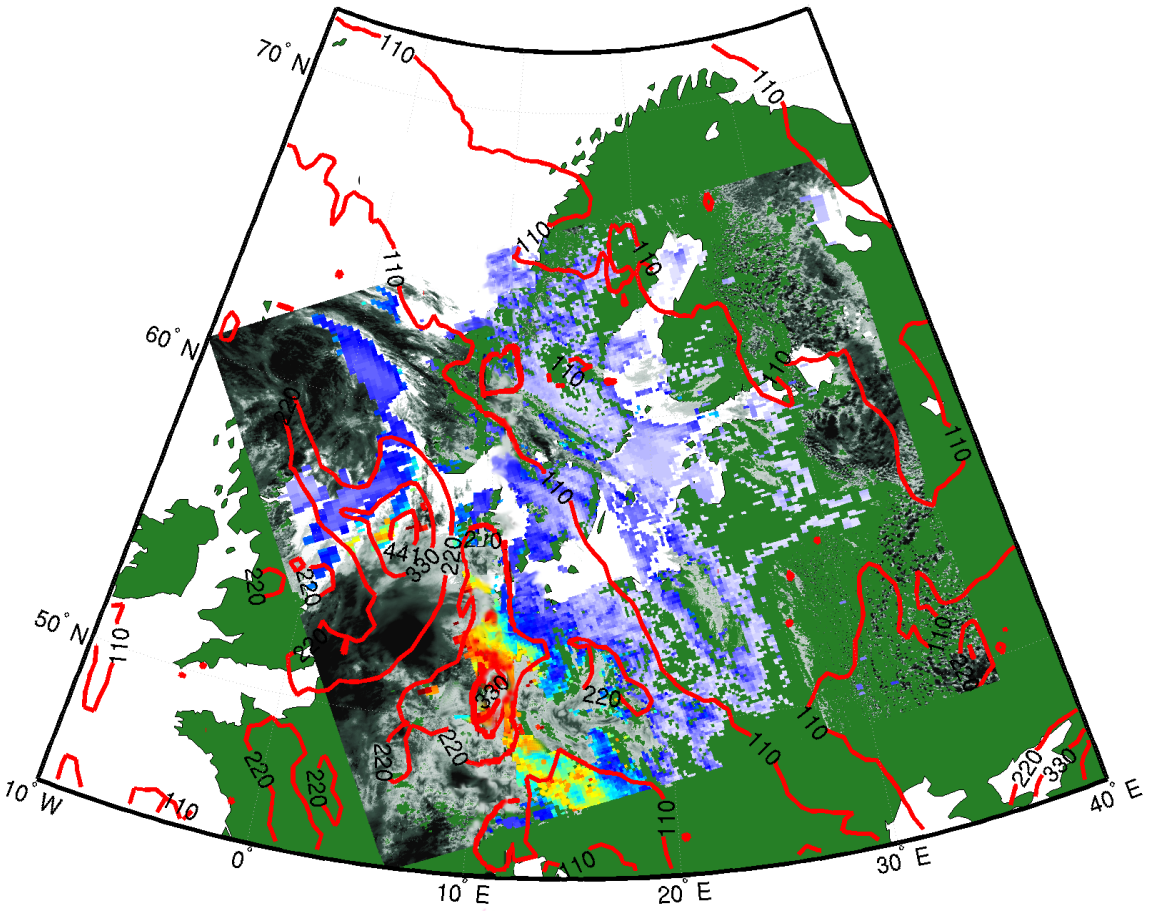

Figure 4.3: Plotted for May 4 2008, are contours of FLEXPART χ_{CO} column concentrations (mg m^{-2}) co-located with MODIS cloud optical depth (gray shading) and MODIS aerosol optical depth (Colored shading) . For cloud free regions, higher values of MODIS aerosol optical depth are associated with hogher values of column χ_{CO} concentrations.

reasonably accurate.

Figure 4.3 shows FLEXPART column χ_{CO} concentration values co-located with MODIS cloud and aerosol properties. In cloud free regions, larger FLEXPART tracer column values are associated with larger aerosol optical depth. Co-locating FLEXPART tracer output with MODIS aerosol retrievals in the Arctic proved to be incredibly difficult. Clouds are extremely ubiquitous in the Arctic and clear sky regions rarely had sufficient amounts of aerosols for the MODIS instrument to detect. An evaluation of the aerosol indirect effect in the Arctic only using satellite retrievals would have a difficult time establishing any sort of relationship between cloud properties and aerosol retrievals from cloud free regions.

4.2 Cloud Height

Establishing the vertical location of both aerosols and clouds is the only way to be able to determine if the two quantities are indeed interacting on a microphysical level consistent with the aerosol indirect effect. MODIS, being a passive radiometer, infers cloud top height from measured radiances and various radiative transfer calculations that use a variety of assumptions (Platnick et al., 2003), one of which is an estimated temperature profile. With the launch of the A-train satellite group, compared to active Cloudsat and CALIPSO height retrievals MODIS typically underestimates cloud top height by with a negative bias of 0.85 ± 1.0 a kilometer or more (Weisz et al., 2007). The large bias arises from using the CO_2 slicing technique that has problems detecting optically thin cirrus and because the strongest radiative signature that MODIS measures originates not from cloud top but deeper within the cloud. However, for low level marine clouds, MODIS uses an 11 μm brightness temperature difference matched to an NCEP estimated atmospheric profile. Holz et al. (2008) identified a positive bias of 1.5 km for the collection 5 MODIS cloud top heights with respect to CALIOP cloud top heights. The algorithm generally chooses the first height from the estimated profile that corresponds to the measured 11 μm brightness temperature. When a temperature inversion is present, the normal situation in the Arctic (Shupe et al., 2006), two heights will correspond to the MODIS 11 μm brightness temperature and the algorithm working from the top down chooses the first height that it encounters (King et al., 2005).

The positive cloud top height bias found by Holz et al. (2008) was in the warm subtropical regions with heavy large scale subsidence known for marine clouds. Since the Arctic is considerably removed from that region both physically and meteorolgically. Using a similar approach as Holz et al. (2008), I compared passive MODIS and POLDER cloud top height retrieval algorithms with the active CALIOP (Cloud-Aerosol Lidar with Orthogonal Polarization) lidar retrievals (Buriez et al., 1997; Platnick et al., 2003; Winker et al., 2009) for cloud scenes typical of what is analyzed in the thesis. The synergy be-

tween the A-train satellite group allows cloud top heights to be temporally co-located for the three instruments. Cloudy scenes were first visually identified to ensure that CALIOP was representing a broad stratus cloud deck then cloud top heights retrievals from MODIS and POLDER were averaged for two pixels adjacent to the CALIOP footprint. The study period spanned the end of March through July 2008 and several cloudy scenes from each month were statistically compared, all of which were over open ocean. For the low-level stratiform clouds that were compared, MODIS cloud top heights were found to have a consistent positive bias of 1.6 $\pm$ 0.5 km compared to POLDER and CALIOP. An important implication of this bias is illustrated in Figure 4.4. MODIS cloud top heights correspond to CO tracer concentrations that are considerably different than the layer where the CALIOP Lidar and POLDER cloud top height retrievals indicate the cloud actually lies.

4.3 Co-location of Satellite Retrievals and Pollution Tracer

Satellite retrieved cloud properties from POLDER and MODIS are provided at different spatial resolutions, MODIS cloud products are provided at 1 km $\times$ 1 km resolutions (nadir) for τ and r_e, while T_c is provided at 5 km $\times$ 5 km resolution (nadir). The POLDER P_{O_2} pressure is derived from 6 km $\times$ 6 km resolution observations but it is provided at a fixed resolution of 20 km $\times$ 20 km. Finally, the synergistic POLDER-MODIS cloud phase product is derived and provided at the full POLDER native resolution of 6 km $\times$ 6 km.

Prior to co-location with the FLEXPART tracer fields, all satellite cloud products are spatially co-located on a fixed resolution sinusoidal grid (equal area) of 6 km $\times$ 6 km to maintain phase information at its highest resolution. Next, these merged POLDER and MODIS cloud products are temporally and spatially co-located with FLEXPART output, where the A-train satellite overpass time is matched to the appropriate FLEXPART tracer field, which is output every three hours. For example, a 833 UTC satellite overpass will be matched up with the 900 UTC FLEXPART pollution tracer fields, which represent an average of tracer concentrations between 600 and 900 UTC. Here, we only evaluate the

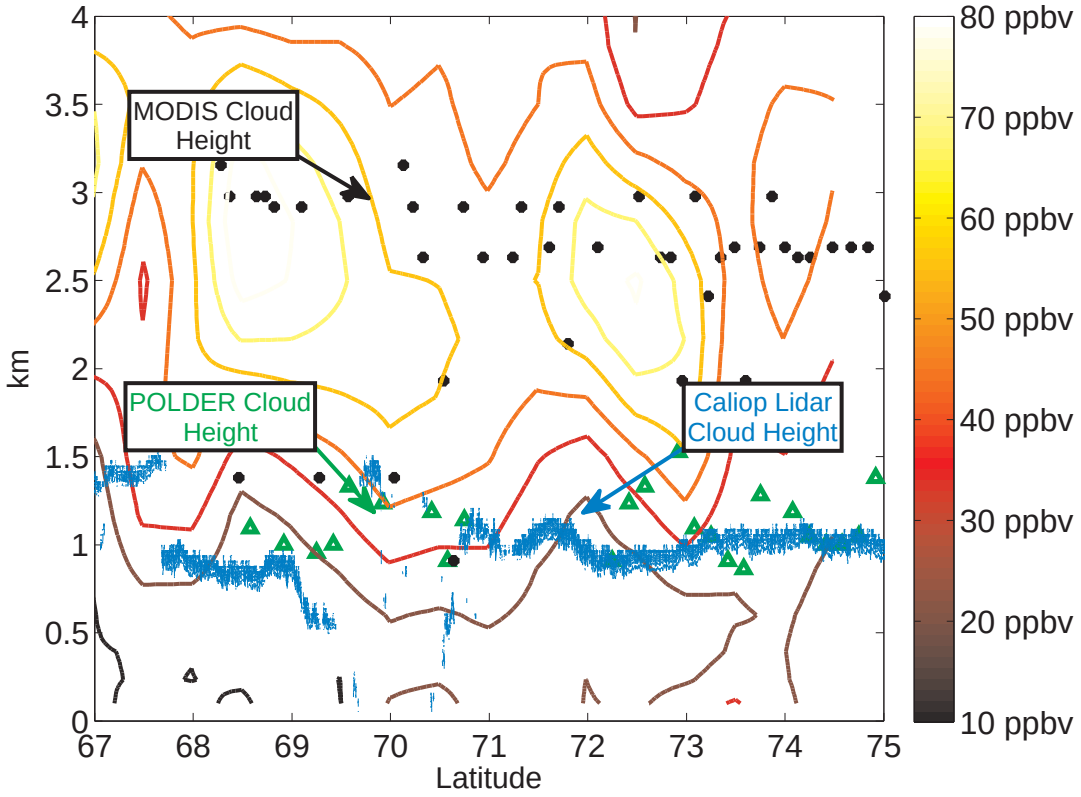

Figure 4.4: Cloud top heights from the A-train instruments MODIS (black dots), POLDER (green Δ) and CALIOP (blue dash), plotted with FLEXPART pollution tracer output (Contours) modeling anthropogenic and biomass burning CO emissions. The figure represents a visually identified stratiform cloud deck in the White Sea.

effects of pollution on low-level Arctic clouds corresponding to POLDER P_{O_2} pressures larger than 800 hPa. Figure 4.5 shows an example of a typical cloudy scene that meets this criteria.

The scheme for horizontal and vertical co-location of pollution and cloud property fields is illustrated in Figures 4.6 and 4.7. FLEXPART concentrations are output for atmospheric layers of roughly 1 km depth in the lower troposphere. Cloud retrievals associated with POLDER P_{O_2} pressures lying within the boundaries of each FLEXPART grid box are compared with the FLEXPART concentrations in that grid box. Clouds with P_{O_2} pressures between 800 hPa and 900 hPa are co-located with FLEXPART concentrations for FLEXPART grid boxes between 1 km and 2 km (e.g. Figure 4.7). Clouds with P_{O_2} pres-

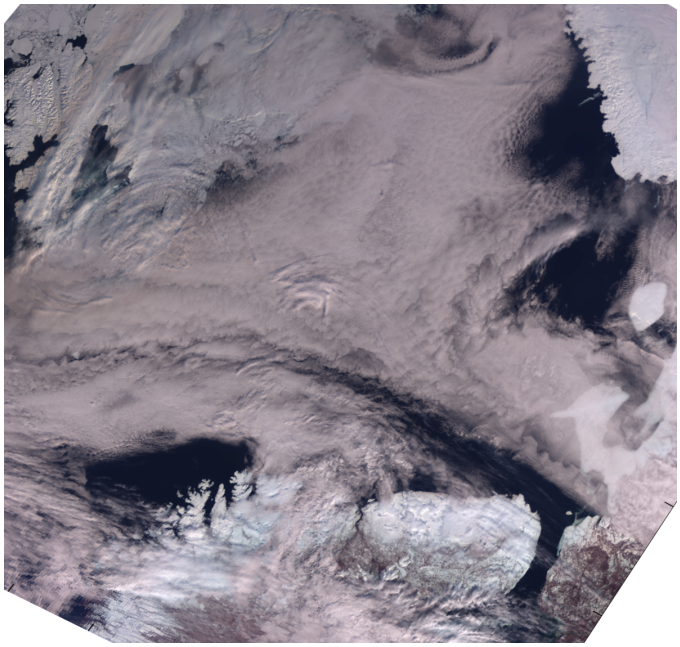

Figure 4.5: True color image of a typical stratus cloud deck in the White sea off the northern coast of Norway and Finland. The image was captured by the MODIS instrument aboard the Aqua satellite on April 28 2008.

sures between 900 hPa and 975 hPa are co-located with FLEXPART concentrations for the grid boxes between 200 m and 1 km.

The $0.5^{o} \times 0.5^{o}$ horizontal resolution of the FLEXPART model grid is considerably coarser than the 6 km $\times$ 6 km satellite derived cloud property retrievals. To account for the disparity in resolutions, an averaging of cloud properties was performed for each FLEXPART three-dimensional grid box, such that each grid box has only one set of cloud property values associated with it. Within each FLEXPART grid box, satellite retrieved properties were averaged together only if all retrievals of the cloud properties considered were successful. For example, if a cloud pixel has a successful cloud top height and effective radius retrieval, but the thermodynamic phase was indeterminate, then none of the properties from the pixel are included in the analysis.

For the atmospheric heights below 800 hPa used in this study, clouds were generally stratiform so that within a typical FLEXPART grid box, the variability in cloud properties was relatively small. Grid boxes with less than 50% cloud coverage within a given

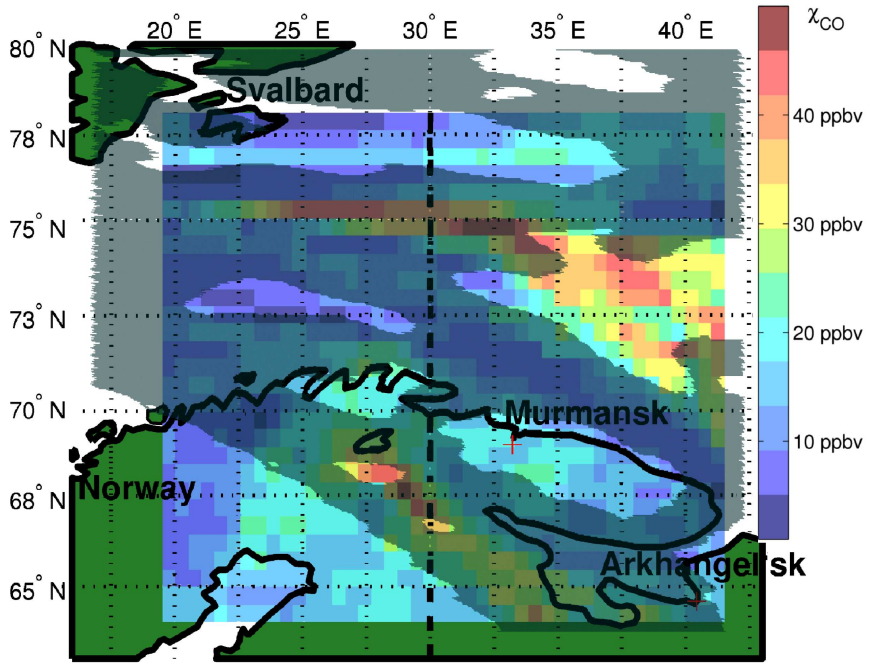

Figure 4.6: Cloud with pressures from POLDER between 800 hPa -900 hPa (gray shading) and average χ_{CO} concentrations in ppbv for a layer between 1 km to 2 km altitude, colored shading. The dotted line is the location of vertical transect shown in Figure 4.2.

FLEXPART level were not used in the assessment of pollution-cloud interactions.

The co-location method is subject to some amount of error and uncertainty affecting the relationship between χ_{CO} and cloud properties. FLEXPART χ_{CO} fields are only output every 3 hours, making the maximum temporal difference between observed cloud properties and pollution to be 1.5 hours. Advection errors from the ECMWF model grids and the parametrized turbulence are also possible. Anthropogenic emission inventories are based on data from previous years, making χ_{CO} emission estimations another source of uncertainty. Furthermore, MODIS is only able to detect biomass burning under relatively cloud free conditions, possibly leading to underpredicted values of biomass burning χ_{CO}. Lastly, although generally minor in Arctic, the FLEXPART model does not take into consideration local sources of aerosols that also are interacting with clouds and observed in cloud structures (Shaw et al., 2010).

These uncertainties in the data retrievals and co-location technique will act to weaken

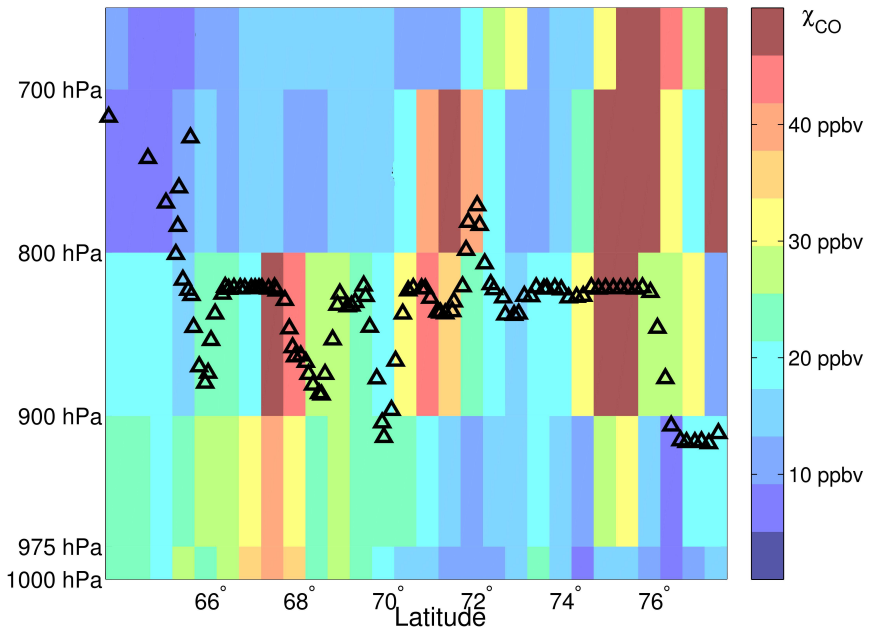

Figure 4.7: Illustration of the vertical co-location method used for satellite data and chemical tracer transport model output. The colors represent values of the CO pollution tracer for a vertical slice along the 30° East meridian. The △ represent the POLDER retrieved cloud top pressure. After co-locating fields of cloud properties both horizontally and temporally, the cloud top pressure is matched to the output of the FLEXPART model that corresponds to the vertical location of the cloud.

the correlation between χ_{CO} and cloud properties and values of IE be fundamentally smaller than for comparisons using simultaneous in-situ measurements of aerosols and clouds. However, by co-locating satellite retrievals with FLEXPART tracer output fields, the analysis approach used here has the major advantage of achieving high statistical coverage of the Arctic while allowing for a climate scale comparison of pollution and clouds under similar meteorological regimes.

CHAPTER 5

RESULTS

Figure 5.1 illustrates the general nature of the liquid clouds that were analyzed over the period between March 20th and July 20th, 2008. More than 80% had cloud top temperatures below freezing, indicating supercooled water droplets. The characteristics of the retrieved cloud properties are, for the most part, consistent with prior in-situ measurements of Arctic stratiform clouds (de Boer et al., 2009). For clouds between 800 to 900 hPa,

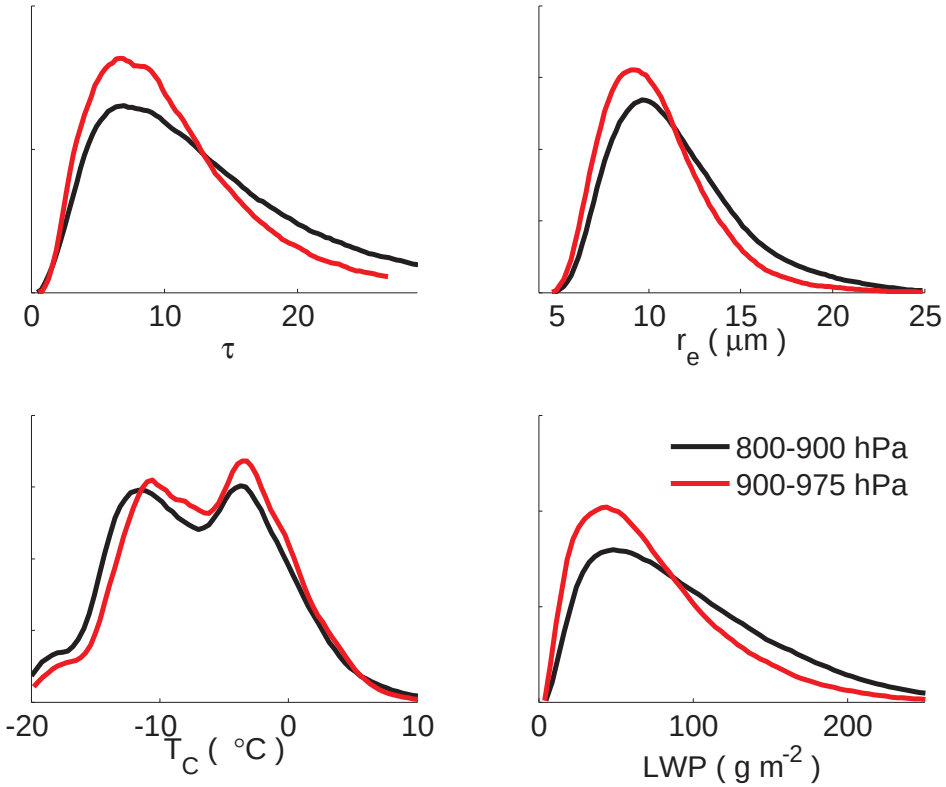

Figure 5.1: Probability distribution functions for the low-level, liquid cloud properties of Arctic clouds north of 65^o N , sampled over the period March 20th and July 20th, 2008.

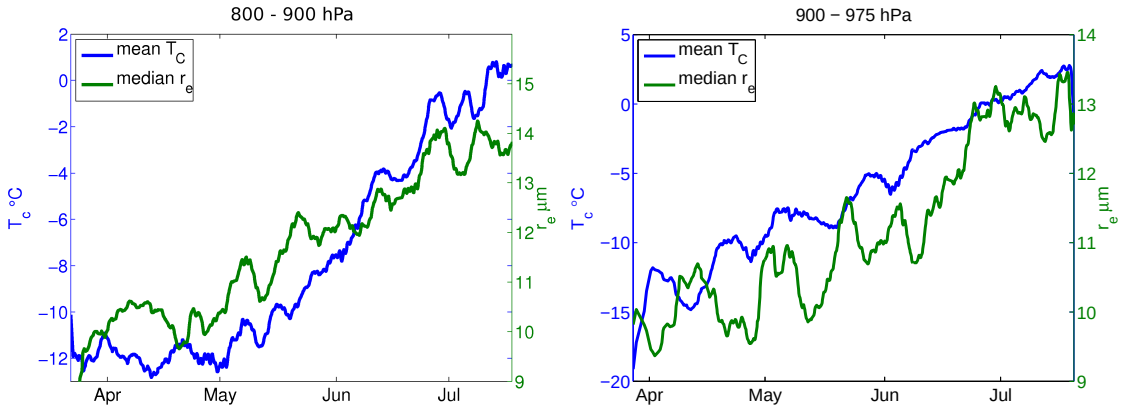

Figure 5.2: Hourly values of mean T_C (°C) and median r_e (μm) for low-level Arctic clouds that were co-located with the pollution tracer in the analysis. Plotted from March 21st through July 20.

median [lower quartile, upper quartile] values for τ are 11.4 [6.9, 17.1], 82.7 g m^{-2} [49.6, 128.2] for LWP and 10.8 μm [8.94, 13.33] for r_e and for clouds between 900 to 975 hPa values are τ 10.0 [6.6 14.5] for τ, 69 g m^{-2} [41.7, 107.3] for LWP and 9.9 μm [8.3, 11.9] for r_e .

Figure 5.2 shows the hourly median r_e and mean T_C for low level liquid clouds used in the study from March 21st to July 20th 2008 separated by 800 hPa to 900 hPa in the upper plot and 900 hPa to 975 hPa in the lower plot. Median r_e values are shown because the distribution of r_e is not a normal distribution and median values better represent typical droplet sizes, while T_C values are much closer to being normally distributed and mean values are plotted. Initially, for the layer 800 hPa to 900 hPa, the mean values for T_C are fairly constant with values near -12 °C until the start of May with a steady rise to about 1 °C at the end of the study. In the lower layer 900 hPa to 975 hPa, values of T_C show a continuous increase from < -15 °C at the start of the study to around 2.5 °C at the end of the study. Values of r_e show a very close relationship with T_C, demonstrating that cloud properties are primarily determined by their meteorological conditions and to a lesser degree by anthropogenic changes in pollution.

Figure 5.3 shows an example of the calculation of IE_{re} (Eq. 2.3), showing a comparison

between FLEXPART χ_{CO} fields and space-based retrievals of retrievals of r_e in low-level liquid clouds. The scatter from the figure indicates that pollution does not have the primary control on r_e and, almost certainly, meteorology has a more significant relationship. However, the large amount of $0.5^\circ \times 0.5^\circ$ data points considered (12,365) enables determination of a weak correlation between high levels of pollution and small effective radii.

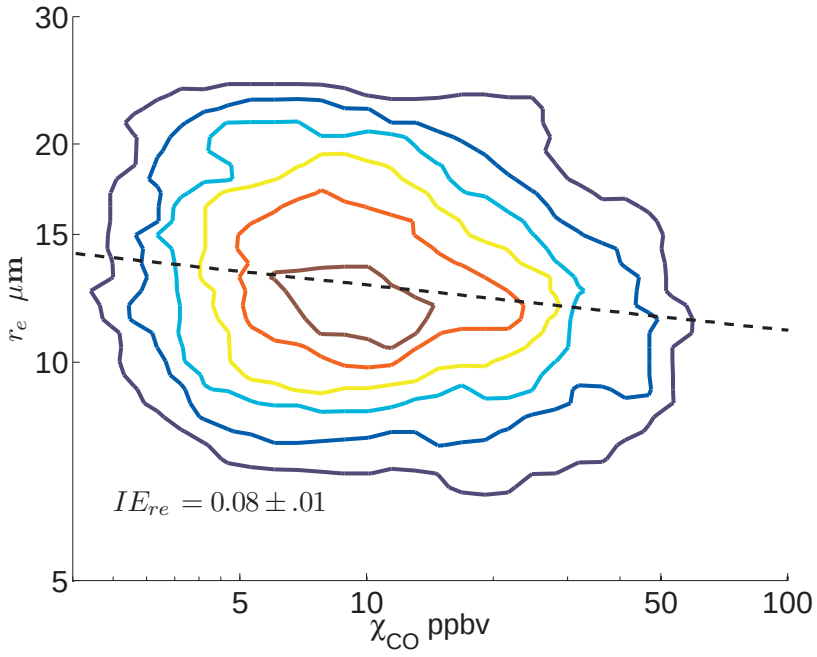

Figure 5.3: Calculation of the IE parameter from a distribution of values of r_e and χ_{CO} for liquid clouds in the Arctic with cloud top pressures between 800 and 900 hPa and cloud top temperatures between 0° C and 2° C.

Figure 5.4 shows the IE parameter (Eqs. 2.7 - 2.9) calculated for small bins (2°C) of temperature and pressure. The plots show that independent of pressure level, there is a general increase in values of IE with temperature until T_C reach 0° C, and lower sensitivity at higher temperatures. Except for the coldest temperatures ($< -6^\circ$ C), the sensitivity is larger for τ than for r_e because changes in χ_{CO} are also associated with changes in LWP. Values of IE are smaller for graybody clouds with LWP < 40 g m^{-2}, than for thicker clouds.

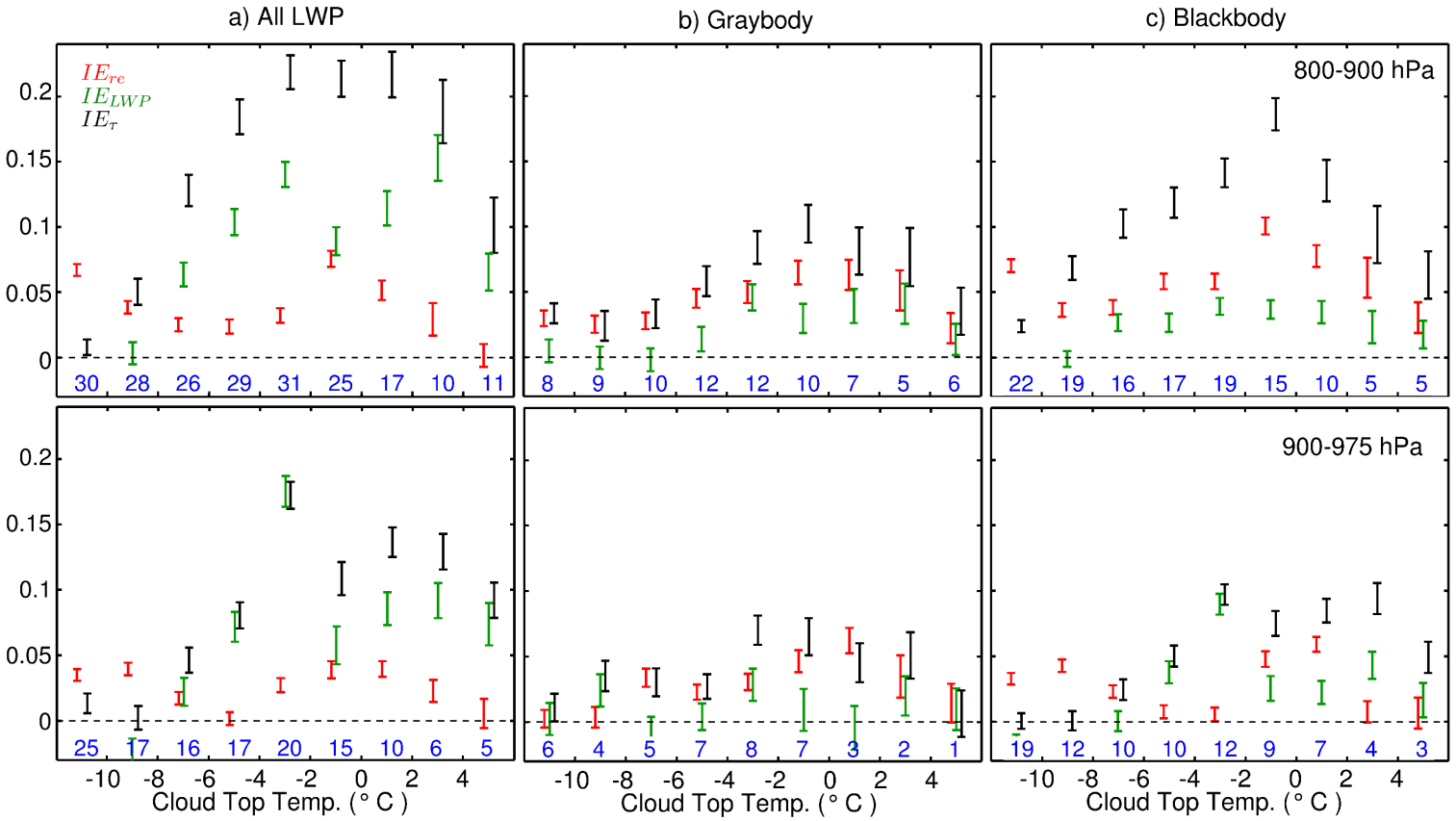

Figure 5.4: IE parameter as a function of temperature calculated for liquid clouds ($\phi < 50$) north of 65° N from March 20 through July 20, 2008 for the layers 800 hPa to 900 hPa (Row 1) and 900 hPa to 975 hPa (Row 2). The bars indicate the 95% confidence limit in the calculation of the fitted slope. The figures are grouped according to; (a) all LWP , (b) graybody clouds with LWP < 40 g m^{-2} or (c) blackbody clouds with LWP > 40 g m^{-2} . Blue numbers indicate how many FLEXPART grid boxes containing clouds, in thousands, went into the calculation of the IE parameter.

Traditionally LWP is constrained to some narrow range when evaluating the first aerosol indirect effect (Twomey, 1977). Here, however, no LWP constraint is initially made in order to allow information to be gained about possible feedbacks that would increase LWP and are usually neglected in aerosol indirect effect studies (Stevens and Feingold, 2009). One constraint of LWP < 40 g m^{-2} is chosen in order to isolate any dynamic feedbacks in clouds that are sufficiently thin to act as graybody emitters (Garrett et al., 2002; Garrett et al., 2009). Clouds emitting as graybodies are hypothesized to be particularly susceptible to aerosol enhancements that create a climatologically significant warming effect (Garrett and Zhao, 2006; Lubin and Vogelmann, 2006; Mauritsen et al., 2010). Once the LWP exceeds 40 g m^{-2} the cloud is an approximate blackbody and cloud longwave emission is determined by temperature changes alone.

Although the IE parameter is a better quantification of pollution-cloud interactions when T_C is held constant, it is still useful to analyze values of IE as a function of time for the study period 5. The Arctic region experiences a major meteorological shift going from spring to summer and the sensitivity of clouds to pollution also likely experiences a shift.

Figure 5.5 and 5.6 show IE_{re} and IE_{τ} calculated in 10-day blocks from March 21 until July 20. Hourly values of mean T_C, median r_e, mean anthropogenic χ_{CO} and mean biomass burning χ_{CO} went into the calculation of the IE parameter. In the layer 800 hPa to 900 hPa, the largest values if IE_{re} and IE_{τ} occur in the early spring, where for March and April values range from 0.09 to 0.21 for IE_{τ} and 0.05 to 0.15 for IE_{re} . Cloud sensitivity to pollution decreases to near zero in May but increases in June and July to values of 0.03 to 0.12 for IE_{τ} and 0.0 to 0.07 for IE_{re} , despite overall lower levels of χ_{CO}. The layer between 900 hPa and 975 hPa, shows a very similar pattern in IE values despite χ_{CO} concentrations to be significantly lower.

Higher values of IE_{re} and IE_{τ} appear, to some extent, related to higher amounts of anthropogenic χ_{CO} as well as to smaller droplets and colder temperatures, however large

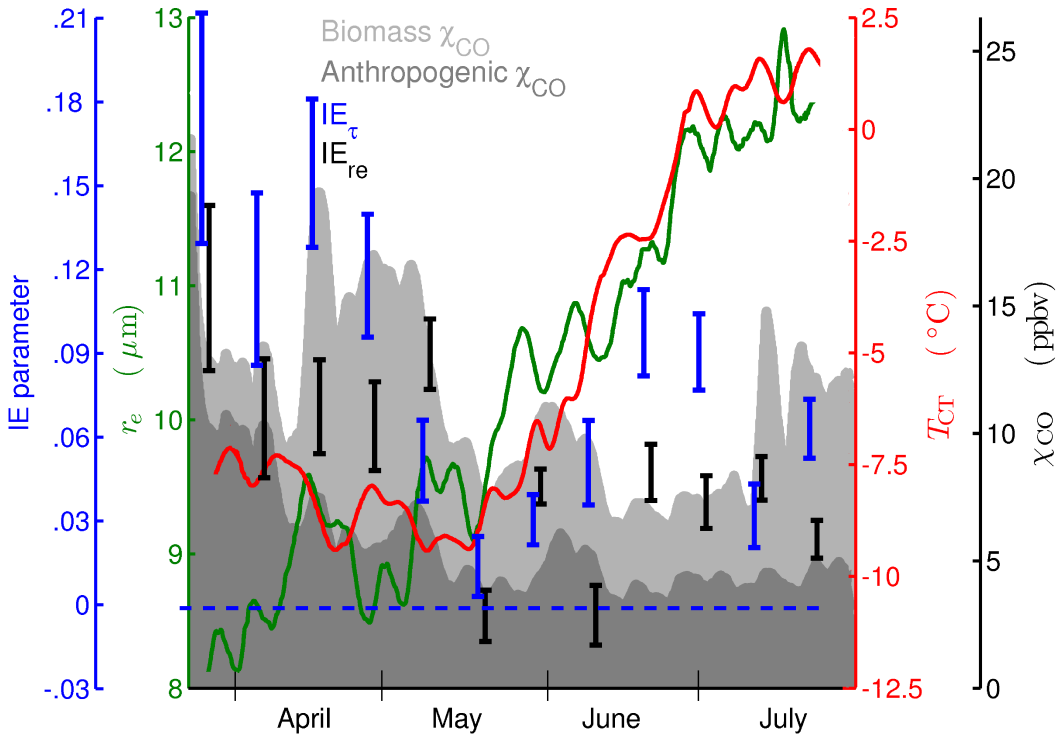

Figure 5.5: IE_{re} (black bars) and IE_τ (blue bars) calculated in ten day blocks March 21^{st} until July 20^{th} plotted with hourly mean T_C and median r_e for clouds used in the IE calculation. Dark gray shading shows Anthropogenic χ_{CO} concentrations and light gray shading shows biomass burning χ_{CO}. Black numbers indicate how many FLEXPART grid boxes containing clouds, in thousands, went into the calculation of the IE parameter.

values of of IE_{re} and IE_τ also occur later in the summer when χ_{CO} is lower and T_C and r_e are both larger. Lastly, values of IE_τ are generally larger than IE_{re} within each ten day block suggesting that LWP is also sensitive to changes in χ_{CO}. Since T_C was not held constant some meteorological bias in IE values is expected to be present where χ_{CO} may be associated with warmer temperatures.

5.1 Biomass Burning

During span of this study, by looking at the individual components of χ_{CO}, we find that biomass burning is clearly affecting the composition of the Arctic lower troposphere, contributing to approximately half of the χ_{CO} concentrations coincident with the clouds that were sampled independent of potential temperature (Figure 5.7).

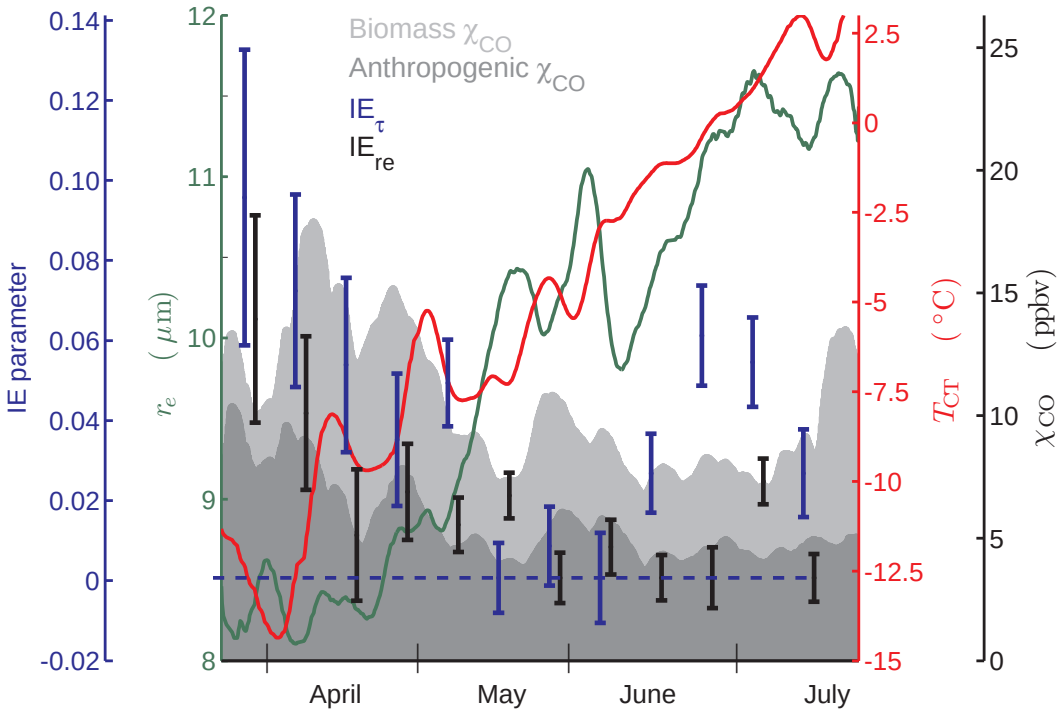

Figure 5.6: Same as Figure 5.5 but for the layer between 900 hPa and 975 hPa. Note the axes scales are different.

Figure 5.7 shows a clear association between larger values of χ_{CO} and warmer potential temperatures θ where $\theta = T(p_o/p)^{2/7}$ and $p_o = 1000$ hPa. This is expected as most pollution originates from lower latitudes and is transported roughly isentropically into the Arctic (Stohl, 2006). Anthropogenic combustion and biomass burning are both sources of CCN and CO (Quinn et al., 2007). Here the ratio of χ_{CO} for the two tracers is near unity in the pollution plumes studied here, but, the chemical composition and relative amounts of ΔCCN for the different tracers are unknown. Aerosols associated with anthropogenic χ_{CO} will not necessarily have equal effects on clouds as aerosols associated with biomass burning χ_{CO}.

The high values of biomass burning χ_{CO} may be explained by large fires occurring at different times during the period of the study. Figure 5.8 shows that the two largest periods of biomass burning impacting Arctic low-level clouds occurred at the end of April into mid May and later again in mid July, two large IPY aircraft campaigns studied and sam-

pled biomass burning plumes during these particular times (Paris et al., 2008; Jacob et al., 2010). Large amounts of Kazakhstan agricultural fires and to a lesser extent Siberian forest fires heavily impacted the ARCPAC study area in April (Warneke et al., 2009). Later in July, biomass burning plumes originating primarily from Siberian forest fires contributed substantially to measured aerosols and trace gases in the Arctic. Figure 5.8 additionally shows that total χ_{CO} concentrations were largest in the early spring and wer almost exclusively anthropogenic until the end of April. During June and July, concentrations are considerably lower than the earlier months indicating that pollution transport to the lower troposphere does see a noticeable reduction by the end of May 2008.

Prior studies suggest that the quantity of CCN per unit CO in pollution plumes is somewhat sensitive to whether the origins are from biomass burning or anthropogenic combustion. For example, from in-situ measurements made near industrial mid-latitude sites

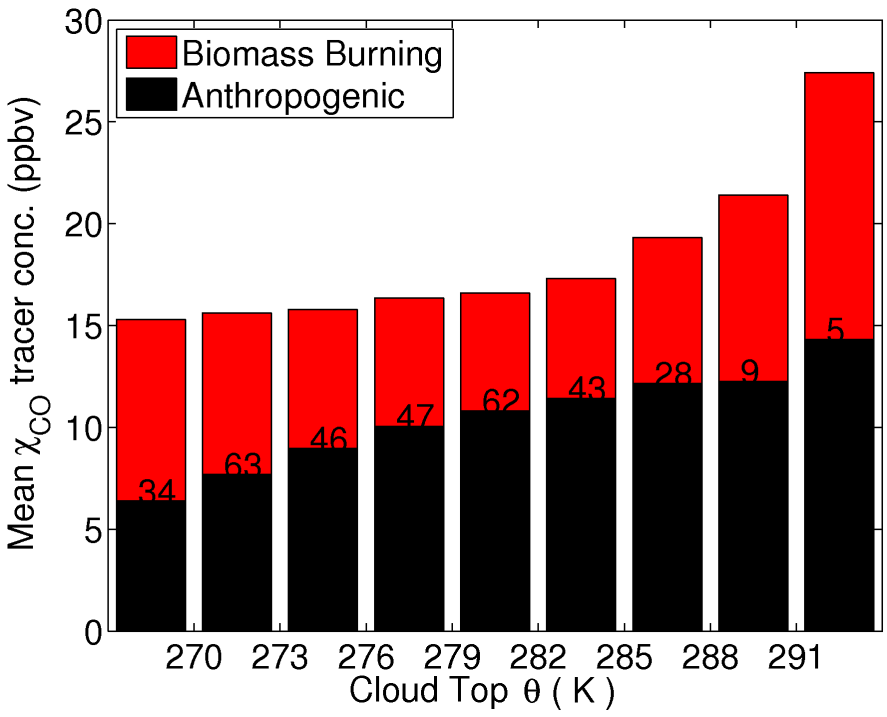

Figure 5.7: Mean χ_{CO} concentrations from anthropogenic and biomass burning sources, for clouds below 800 hPa, binned by cloud top potential temperatures shown on the bottom axis. Numbers, in thousands, indicate how many FLEXPART grid boxes with liquid clouds, at that potential temperature, were averaged together.

in North America and Europe, the ratio of ΔCCN/ΔCO is roughly 25 $\pm$ 15 cm^{-3} ppb^{-1} (Longley et al., 2005; Garrett et al., 2006). Comparable values (40 $\pm$ 20 cm^{-3}ppb^{-1}) can be computed for Arctic haze by relating observed ratios of droplet number concentrations to aerosol light scattering (σ) that are 100 $\pm$ 50 cm^{-3} Mm^{-1} (Garrett et al., 2004) to observations from the same location of $\Delta\sigma/\Delta$CO, which are 0.4 $\pm$ 0.1 Mm ppb^{-1} (Garrett et al., 2010). For recent pollution events χ_{CO} is a good approximation for ΔCO, so that anthropogenic ratios of ΔCCN / χ_{CO} are assumed to be similar to previous observations. Estimating a ratio of biomass burning ΔCCN / χ_{CO} is more difficult because fuel type and fire size play a large role in the aerosol and mass concentration and solubility of its particles (Rivera-Carpio et al., 1996). Large Siberian boreal forest fires are a major but episodic source of aerosol during the spring and summer (Stohl, 2006). Unfortunately, the remote

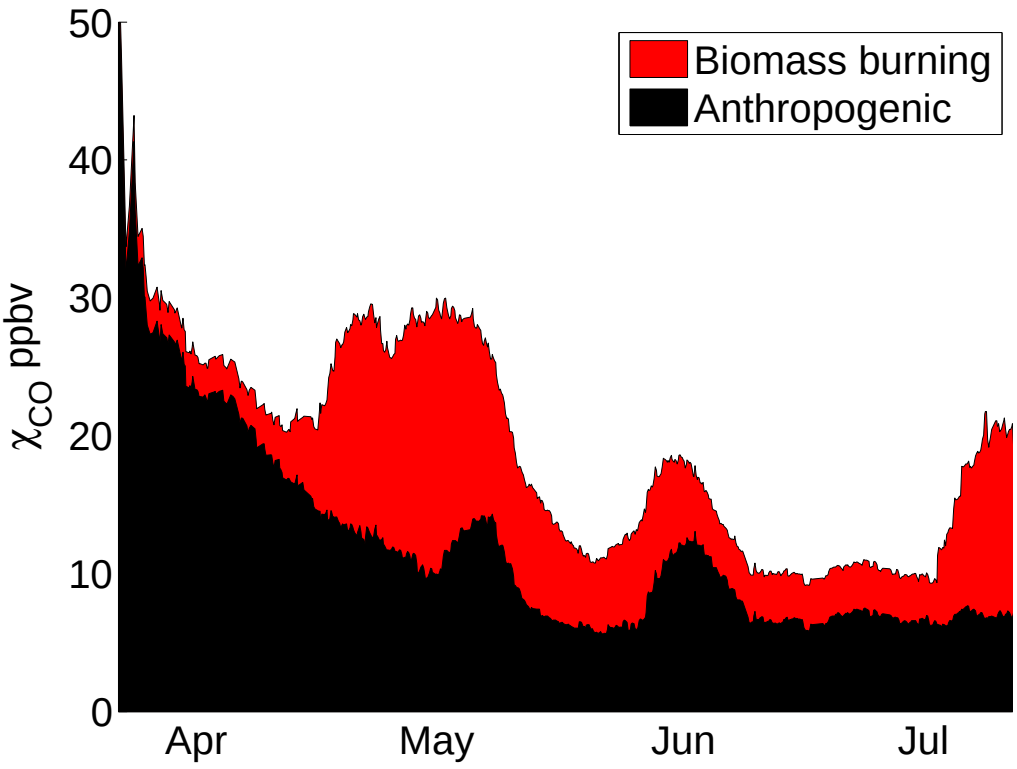

Figure 5.8: Time series of χ_{CO} [ppbv] tracer concentrations coincident with liquid Arctic clouds north of 65° Latitude, in the atmospheric layer between 800 hPa and 900 hPa

region is lacking in studies of biomass burning CCN emission characteristics (Paris et al., 2008). Although regionally distinct, the scale and scope of Siberian Boreal forest fires are similar to large tropical fires previously studied (Andreae et al., 2004; Vestin et al., 2007) where ΔCCN/ΔCO values of 10 ± 2 cm^{-3}ppb^{-1} were observed near the active fires.

In transit to the Arctic, biomass burning and anthropogenic pollution plumes are subject to removal of CCN by wet scavenging. Still, the pollution plumes should retain characteristics of the emission source and influence cloud properties proportional to their composition at emission. On account that ΔCCN / χ_{CO} is potentially a factor of two (or more) larger for the anthropogenic tracer, we investigate the dependence of cloud sensitivity to pollution type, by calculating values of IE for clouds where biomass burning χ_{CO} concentrations were either > 80% or < 20% of the total χ_{CO} concentrations (Figure 5.9). However, the actual ratios of ΔCCN/ΔCO and the chemical composition of the aerosol mass will be different and influence the response of cloud microphysical properties to pollution plumes. To investigate the dependence of cloud sensitivity to pollution type, we calculated values of IE for clouds where biomass burning χ_{CO} concentrations were either > 80% or < 20% of the total χ_{CO} concentrations (Figure 5.9). These values are chosen because pollution plumes will generally be a mixture of both tracers and the effects of just biomass burning cannot be completely isolated.

Figure 5.9 shows that cloud sensitivity to χ_{CO} is only weakly dependent on pollution type. When biomass burning χ_{CO} concentrations are relatively high, Arctic cloud properties show a sensitivity to pollution plumes that is on average lower but still comparable to when the anthropogenic tracer dominates. The primary difference is that biomass burning has a smaller impact on cloud optical depth but sensitivity can still be large for plumes that lie along isentropic surfaces between 282 K and 291 K. Also, r_e shows increased sensitivity to plumes at colder potential temperatures (< 276 K) compared to anthropogenic dominated pollution.

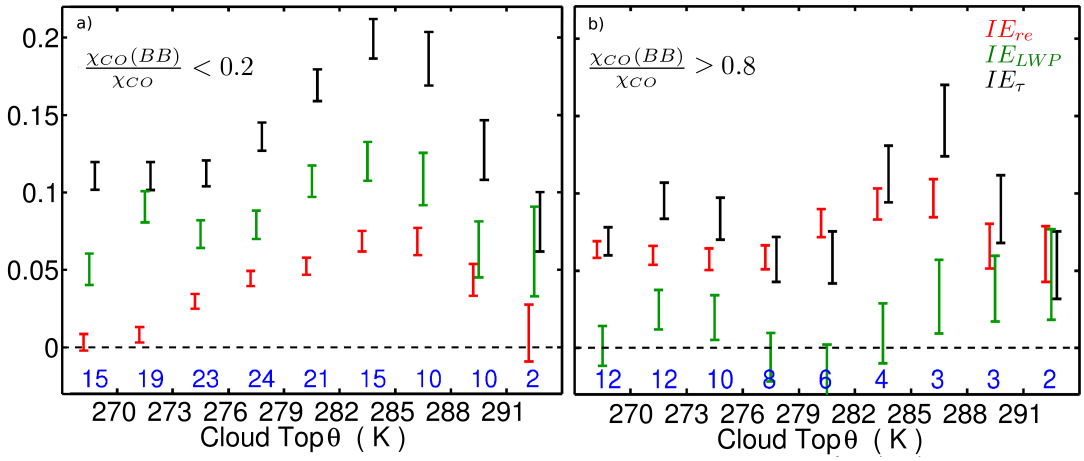

Figure 5.9: As with Figure 5.4, except that the plots represent values of IE for clouds coincident with biomass burning χ_{CO} concentrations that are either > 80% (a) or < 20% (b) of the total χ_{CO} concentrations.

CHAPTER 6

DISCUSSION

6.1 Aerosol Indirect Effect on Arctic Clouds

For low-level, liquid stratiform clouds north of 65° Latitude, from March 20 through July 20, 2008, calculated values of the IE parameter with respect to a pollution tracer range from 0.0 to 0.08 with respect to effective radius (r_e) and 0.0 to 0.17 with respect to optical depth (τ). The largest values of IE occur for temperatures near freezing (Figure 5.4).

For comparison, using ground based measurements obtained near Barrow Alaska, Garrett et al. (2004) found values of IE_{re}, for low-level liquid clouds, in the range of 0.13 to 0.19 when the aerosol quantity considered was light scattering of submicron aerosol. Lihavainen et al. (2009) using a Forward Scattering Spectrometer Probe (FSSP) and Differential Mobility Particle Sizer (DMPS) to directly measure cloud and aerosol properties from northern Finland. They found IE_{re} values of 0.2 to 0.3 when the sampled aerosol sizes were constrained to be between 50 and 150 nanometers and the LWP was constrained between 100 gm^{-2} and 200 gm^{-2} . For the same region and LWP constraints, Lihavainen et al. (2009) related aerosol optical depth, cloud optical thickness and cloud effective radius from satellite measurements to obtain values of ~ 0.1 for both IE_{re} and IE_{τ} .

Satellite based studies have obtained similar values globally, ranging from 0.02 to 0.20 for continental clouds (Nakajima et al., 2001; Feingold et al., 2003; Lohmann and Feichter, 2005; Myhre et al., 2007) and 0.09 to 0.13 for oceanic clouds (Bréon et al., 2002; Sekiguchi et al., 2003; Kaufman et al., 2005; Myhre et al., 2007). Costantino and Bréon (2010) used simultaneous measurements from several active and passive A-train instruments to

investigate the correlation between clear sky aerosol loading and adjacent cloud droplet radius values. Using the CALIOP lidar from the A-train, Costantino and Bréon (2010) were able to determine when African biomass burning aerosol layers were likely coincident and interacting with shallow marine stratocumulus clouds and found IE values of 0.24. However, if there was no indication that aerosol layers were coincident with clouds, the IE value fell to 0.04, demonstrating the importance of vertical and horizontal co-location of aerosol and cloud in studies of the aerosol indirect effect.

Here, comparisons were not made with respect to an aerosol quantity but rather to a passive pollution tracer χ_{CO}. Since concentrations of χ_{CO} are independent of clouds and only affected by dilution and mixing, when the IE parameter is large, the implication is that χ_{CO} concentrations are associated with significant concentrations of CCN that have the capacity to perturb cloud properties. It is no surprise then that the largest values of IE are similar to those obtained in previous studies, because it suggests values of the scavenging parameter, S (Eq 2.7) are close to unity. Values of IE and S are, in general, substantially smaller, when T_C is greater than 2 ^oC, suggesting that at warm temperatures, wet scavenging is sufficiently efficient to limit the effects of pollution plumes on cloud properties. When temperatures are warm enough to support drizzle and rain processes, CCN are efficiently removed from the pollution plumes (Garrett et al., 2010), reducing the sensitivity of clouds to pollution plumes themselves. Why the reduction in sensitivity occurs at $T_C > 2$ ^oC and not 0 ^oC, is not entirely clear and may be a result of slightly inaccurate satellite retrievals, or possibly drizzle processes are more efficient at warmer temperatures. It would be interesting to see how robust this "scavenging point" is in additional analyses.

A similarly low sensitivity to pollution plumes is found at cold temperatures below -6°C. It is unclear why the sensitivity of cloud microphysics to pollution is so low at cold temperatures; wet scavenging is unlikely to be particularly efficient due to low precipitation rates. Perhaps the supersaturations found in these cold clouds are too low to activate pollution aerosols and increase cloud droplet concentrations. What is more likely is that cold

air masses have longer transport times from mid-latitude pollution source regions (Stohl, 2006) and the time-integral of precipitation rates is what ultimately determines the extent of wet scavenging. This may explain the "inverted-U" shape in the IE signature shown in Figure 5.4, where competing effects of low precipitation but long transport times at cold temperatures lead to low IE values at cold temperatures while short transport times but high precipitation at warm temperatures. leads to the other minimum. Thus, the maximum value of IE likely occurs where the time integral of precipitation rates along transport pathways is at a minimum.

The increased sensitivity of τ over r_e to pollution is an an interesting result of the study and may be a result of the broad statistical nature of the data sampling that allows for the effects of possible dynamical and microphysical feedback processes occurring on short time scales to be evident in the analyses. If LWP is unaffected by pollution and S is low, then the IE parameter calculated with respect to r_e and τ will be approximately equal (see Eq. 2.5), and absent any dynamical feedbacks, IE values will range between 0 and 0.33 (Feingold, 2003). Here, IE is calculated by empirically fitting a slope to data that encompasses many phenomena in a complex system. Since the data sampling occurs at various stages from cloud formation to dissipation and over a long time period, the results will include information about any dynamical feedback or precipitation process that may mediate the overall cloud response to pollution (Stevens and Feingold, 2009).

Figure 6.1.1 shows observed values of an enhancement factor (EF) representing the degree to which the cloud optical depth sensitivity IE_τ exceeds the droplet effective radius sensitivity IE_{re} based on results in shown in Figure 5.4, and plotted against potential temperature. When no constraint is made on LWP, values of EF are about four for values of $\theta > 273$ K. The magnitude of the enhancement factor is smaller by about a factor of two when LWP is constrained to graybody clouds or blackbody clouds and when biomass burning is greater than 80% of the total χ_{CO} concentrations .

Values of EF range from a factor of 1 to 4.5. The magnitude of the enhancement

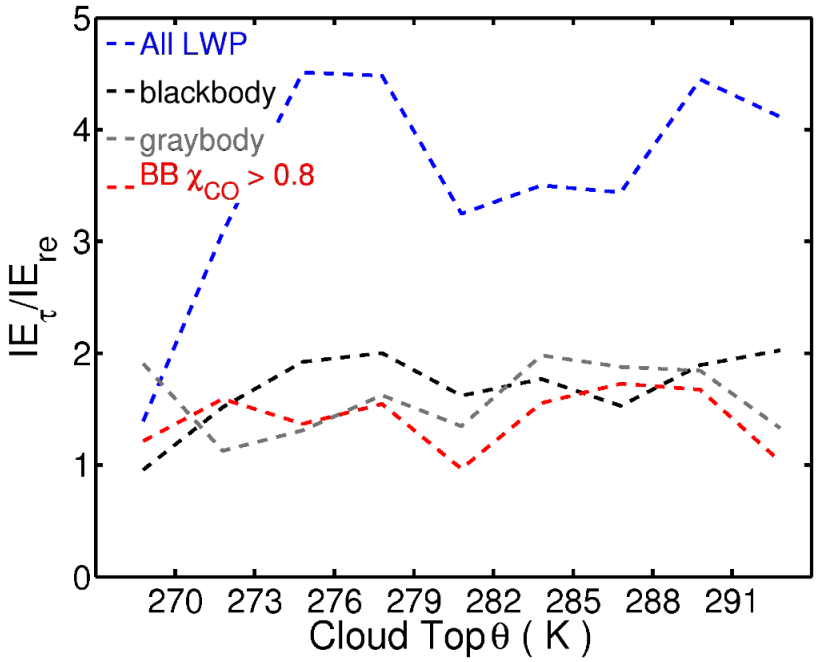

Figure 6.1: Enhancement of IE_τ over IE_{re} as a function of potential temperature, θ(T_{CT}, P_{O_2}) for low-level liquid clouds in the Arctic from March 20 to July 20, 2008. The enhancements are plotted according to; (blue) all LWP, (gray) graybody clouds with LWP $<$ 40 gm^{-2} , (black) blackbody clouds with LWP $>$ 40 gm^{-2} or (red) BB χ_{CO} > 0.8 of the total χ_{CO} concentrations.

for blackbody, graybody, and clouds dominated by biomass burning χ_{CO} is half that of when no constraint is made. If no change in LWP was associated with changes in pollution then by Eq 2.1the τ would have an equal sensitivity to pollution as r_e, so clearly some aspect of pollution is affecting LWP. The observed EF's are robust in the sense that for all potential temperatures bins, pollution types and different LWP subsets there is some amount of increased sensitivity of τ over r_e to pollution. Campaign values of IE for various subsets of data allows some determination of the physical processes occurring.

Enhancement at low LWP for graybody clouds may be indicative of the radiative feedback process that accelerates cloud development when thin clouds are polluted (Garrett et al., 2009). Specifically, cloud thermal emissivity is a function of droplet size when the

LWP is below 40 g m^{-2} (Garrett et al., 2002). When these graybody clouds are polluted, the thermal emissivity increases, adding an extra flux of longwave energy to the surface compared to clean clouds (Garrett and Zhao, 2006; Lubin and Vogelmann, 2006). Furthermore, a feedback arises because the polluted cloud also increases its thermal emission at cloud top, which increases the radiative flux divergence, the mechanism driving condensate production, the cloud thickens which in turn enhances cloud top radiative cooling. This process only applies to thin graybody clouds because at LWP greater than 40 g m^{-2} thermal emissivity is only a function of temperature alone. Since large enhancements of EF occur for clouds with large LWP, other mechanisms must also contribute.

Precipitation and evaporation are the sinks of cloud condensate and will directly control LWP. For liquid phase clouds, smaller droplet sizes tend to reduce drizzle and warm precipitation by inhibiting collision-coalescence processes (Albrecht, 1989). All else being equal, this would lead to an enhancement of liquid water path and a long-term thickening of liquid stratiform clouds(Baker and Charlson, 1990; Pincus et al., 1997). A feedback could occur because precipitation is also the major sink of aerosol particles, thus allowing aerosols to persist, further inhibiting precipitation and lengthening the cloud lifetime. However, in a dynamically active system, all else tends not to be equal. An increase in LWP due to precipitation suppression may be canceled out or reduced by other compensating and concurrent dynamic processes (Wood, 2007; Stevens and Feingold, 2009). Further constraints and observations of precipitation are needed before any conclusions of precipitation suppression is leading to the observed enhancement of LWP.

Also, a common but tenuous regime of supercooled liquid clouds precipitating ice is frequently observed in the Arctic (Curry et al., 1996; Intrieri et al., 2002; Shupe et al., 2006). Using a mesoscale computer model to simulate Arctic clouds, Morrison et al. (2008) found that in the Arctic, elevated aerosols concentrations reduce riming processes and this can lead to increased LWP and cloud lifetime because ice particle growth is inhibited and suppresses ice crystal precipitation. By restricting the analysis to clouds with a radiatively

determined phase index of $\phi < 50$, the study likely did not exclude liquid clouds that were precipitating ice. Thus, this feedback potentially is contributing to the observation of LWP sensitivity to pollution, although it would not explain large enhancement values (EF) at temperatures > 0°C (Figure 6.1).

A correlation between CO and LWP may also be expected for dynamical reasons. As a polluted mid-latitude and, thus, relatively warm air mass intrudes into the Arctic, it typically rises slantwise along a frontal surface above the colder Arctic air. A cloud formed in such an air mass may be expected to be deeper than an average Arctic cloud considered in our analysis. The impact on the result shown here is minimized by controlling our analysis for both cloud top temperature and pressure and considering only stratiform clouds with cloud tops below 2 km, whose depth is clearly limited. Still, the effect may partly explain why IE_{LWP} values are larger than IE_{re} values.

6.2 Influence of Biomass Burning on Arctic Clouds

Biomass burning clearly contributes significantly to total pollution levels affecting low-level liquid clouds in the Arctic (Figs 5.7 and 5.8), consistent with results from several ARCTAS related studies during April 2008. Compared to when anthropogenic pollution dominates the plumes, when biomass burning dominates, cloud optical depth shows a similar but reduced sensitivity to pollution, while r_e shows a similar but slightly higher sensitivity, particularly at colder temperatures (Figure 5.9). This is interesting given that all else being equal, one would expect anthropogenic pollution plumes to have a significantly larger impact on cloud properties due to the larger proportion of highly soluble CCN to CO (Bower and Choularton, 1993) while biomass burning plumes typically contain CCN that are a mixture of soluble and insoluble particles activating at a much larger range of supersaturations and have a smaller ratio of ΔCCN/ΔCO (Rivera-Carpio et al., 1996; Pradeep Kumar et al., 2003; Vestin et al., 2007).

Large amounts of biomass burning χ_{CO} were observed coincident with clouds during

end of June and into middle July (Fig. 5.8), when aerosol removal mechanisms, both wet and dry deposition, are thought to be considerably more efficient (Garrett et al., 2010). Yet, there is still a significant sensitivity of Arctic clouds to χ_{CO} during this time (see Figs. 5.5 and 5.6). The high sensitivity of τ may be an indication of the second aerosol indirect effect (Albrecht, 1989) where precipitation and wet removal is suppressed by the high aerosol number concentrations. This phenomena has been observed in tropical biomass burning regions (Andreae et al., 2004) where, in the vicinity of the large fires, precipitation is inhibited allowing stronger convection to occur and enhanced transport of biomass burning aerosols. Although the same microphysical arguments apply to the Arctic biomass burning plumes, the dynamical meteorological conditions and biomass types significantly different, preventing easy application of their results here.

Another possibility as to why there is a high sensitivity of τ and to a lesser extent, r_e, to biomass burning during these times is that during the relatively clean summer a tenuous cloud regime develops where cloud formation is limited by available CCN rather than moisture flux convergence (Mauritsen et al., 2010). In this tenuous cloud regime, clouds will be especially sensitive to small changes in CCN concentrations, such that even if the majority of cloud active particles are scavenged from the χ_{CO} pollution plumes, there will still remain sufficient quantities of CCN to create a discernable impact.

However, observations may be slightly biased if this tenuous low CCN regime is indeed present. Here, the analysis procedure is to observe clouds first, then compare their properties to the fields of χ_{CO}. If cloud formation is limited by CCN, then they are more likely to form in pollution plumes that still contain CCN. It may be that the vast majority of pollution plumes entering the Arctic in the summer have already been depleted of CCN and no cloud formation is associated with those pollution plumes.

Additionally, the minimal enhancement in values of IE_τ over IE_{re} observed in biomass burning dominated pollution is surprising and may be indicative of other radiative characteristics of biomass burning aerosols dampening feedback processes affecting LWP. This

study only examined the influence of biomass burning plumes on co-located clouds. It did not preclude situations where biomass burning layers may be situated above the cloud layer. During the late spring and summer these layers would strongly absorb shortwave radiation and add an additional thermal forcing at cloud top (Brioude et al., 2009). The added warm layer may increase the atmospheric stability and favor low cloud development or conversely, the added thermal flux may decrease the relative humidity and enhance evaporation, dissipating the cloud (Klein and Hartmann, 1993).

Lastly, interactions with shortwave radiation by absorbing aerosols contained within biomass burning plumes may create inaccuracies in satellite cloud property retrievals (Platnick et al., 2003; Rosenfeld and Feingold, 2003). While we show an overall sensitivity of cloud properties to biomass burning plumes, a closer examination of the vertical profile and thermal characteristics of the biomass burning tracer is needed in order to constrain these possible effects.

CHAPTER 7

SUMMARY AND FUTURE WORK

This thesis shows how comparisons of spaced-based cloud retrievals with an inert passive tracer from a tracer transport model can be used to quantify the indirect effects of anthropogenic and biomass burning pollution plumes on the properties of low-level liquid clouds in the Arctic. By comparing modeled passive pollution tracers to vertically and horizontally co-located satellite cloud property retrievals, this relieves some uncertainty and meteorological biases seen in previous space-based studies that compare aerosols and clouds from different locations and heights.

A comprehensive analysis of pollution plumes affecting the Arctic region from March 20 to July 20, 2008 shows effects of pollution plumes on clouds that are generally of similar magnitude to previous satellite studies that looked explicitly at the effects of measured aerosols on clouds in lower latitude regions. What differs is that the highest correlation between cloud optical depth, droplet effective radius and pollution occurs at temperatures near freezing, with a decrease in sensitivity at warmer and colder temperatures. An explanation for the decrease at warmer temperatures is that wet scavenging of CCN becomes rapidly more efficient as seasonal temperatures warm. The sensitivity of cloud properties to pollution is only weakly dependent on whether the pollution is primarily anthropogenic or biomass burning in nature. In general, the cloud optical depth has a substantially higher sensitivity to changes in pollution levels than can be explained by changes in cloud droplet effective radius alone. This result occurs at very low liquid water paths as well as large liquid water paths, suggesting that either precipitation suppression or some unknown feed-

back mechanism increases liquid water path and this causes large enhancements of the first indirect effect of aerosols on low-level Arctic liquid clouds. This enhanced sensitivity is less apparent when biomass burning dominates pollution levels.

While this thesis shows clear evidence of both biomass burning and anthropogenic pollution having a significant effect on cloud properties, many questions and uncertainties about the physical processes occurring persist, allowing ample opportunity for further research. Three major themes have a significant impact on the results presented here and can be realistically addressed with further research efforts. Primarily, the precise process that determines the role of wet-scavenging and precipitation in pollution-cloud interactions of Arctic clouds is still rather uncertain. Secondly, biomass burning is a major source of pollution and trace gases in the Arctic, and it appears emissions from biomass burning affect clouds differently than emissions from anthropogenic combustion. A closer examination of the biomass burning pollution is needed to determine why. Lastly, the Arctic is a unique meteorological environment and the limited physical understanding of how clouds influence and interact with the Arctic climate system inhibits any attribution of anthropogenic induced changes.

The different sensitivity of cloud optical depth and droplet effective radius to pollution plumes is of particular interest, as it suggests that certain feedback processes are enhancing the optical depth through changes in the cloud's liquid water path. For warm liquid phase clouds, smaller droplet sizes tend to reduce precipitation by inhibiting collision-coalescence processes (Albrecht, 1989), all else being equal, this would lead to an enhancement of liquid water path, since precipitation is the major sink of cloud condensate. A feedback could occur because precipitation is also the major sink of aerosol particles, thus allowing aerosols to persist and to further inhibit precipitation (Baker and Charlson, 1990). Coupling information about precipitation into the analysis would allow some constraint on this feedback process.

Unfortunately, the remoteness of the Arctic and the low precipitation rates there limit

the amount of available precipitation information that could be easily incorporated into this study. The synergy of the A-train satellite allows for one possible avenue into studying pollution-cloud-precipitation interactions in the Arctic. Two active remote sensing satellites, CloudSat and CALIPSO, allow for the determination of the presence of precipitation and to some extent the actual rate of precipitation. These active satellites could potentially be used to discriminate precipitating clouds from nonprecipitating clouds and a comparison of cloud sensitivity to pollution between the two groups may allow some indication of a precipitation feedback. A passive tracer like χ_{CO} is especially useful here, since concentrations will be unaffected by any feedback process.

The major limitation to this approach is the small spatial resolution of CloudSat and CALIPSO. By constraining the comparison to low-level stratiform clouds and assuming the cloud mass was horizontally unifrom, the satellite precipitation data can be extrapolated to adjacent passive retrieved cloud property data with some degree of confidence. This strategy was used successfully by Kubar et al. (2009) to characterize macrophysical and microphysical properties associated with warm marine drizzling clouds. A similar analysis utilizing co-located pollution tracer data could be used to help determine a relationship between precipitation and pollution, however, different sensitivities to pollution between precipitating and nonprecipitating clouds would not necessarily imply a causal relationship. Precipitation is not the only sink of cloud water; evaporation of cloud droplets and entrainment of adjacent air parcels also affects the total water content (LWP) of the cloud (Figure 7.1). The additional meteorological information from active satellite remote sensing and re-analysis data from NCEP or ECMWF would help isolate the physical processes that are occurring.

Alternatively, to better understand wet scavenging, a similar analysis can be performed on smaller regional scales along known pollution pathways into the Arctic. Comparing the sensitivity of cloud properties to pollution at increasing distances from the source would give some indication on the rates of wet scavenging. Meteorological variability would

have to be constrained and the use of the merged MODIS-POLDER phase product would be particularly useful here, since warm rain is much more efficient at removing aerosols than ice-phase precipitation. The results could be compared to more isolated mid-latitude regions with small pollution gradients to test whether differences in meteorology between the Arctic and mid-latitudes influences cloud properties.

Sensitivity studies using Large Eddy Simulator (LES) type cloud models offer the best opportunity to understand the physical processes related to the observations shown in the thesis, where the effects of precipitation feedbacks and biomass burning pollution can be individually isolated (Morrison et al., 2008; Garrett et al., 2009). An LES model can be run using initial conditions similar to the Arctic clouds studied here and various parameters and variables can be changed to mimic different polluted and clean conditions. A study of how precipitation is affected during the evolution of different modeled cloud regimes,

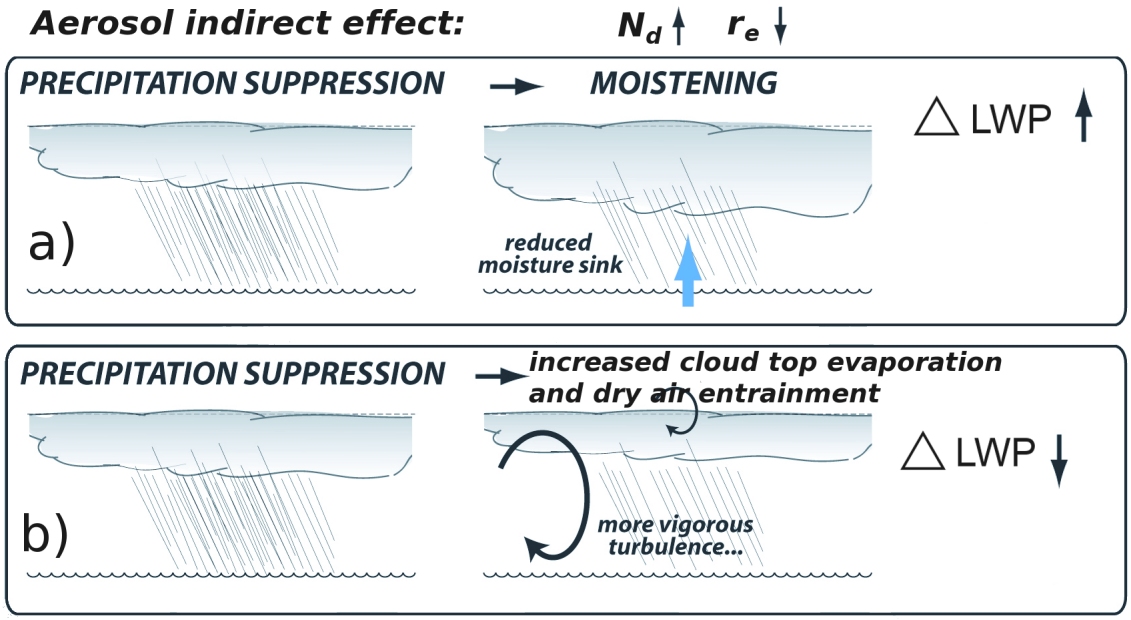

Figure 7.1: Possible cloud macrophysical changes associated with increased cloud droplet number concentrations and reduced droplet sizes from the aerosol indirect effect. When precipitation processes are inhibited by the aerosol indirect effect and evaporation is unaffected cloud LWP increases due to the reduced sink [a)]. However, more numerous smaller droplets have a larger surface area which may enhance cloud top evaporation, increase the entrainment of dry air and reduce the cloud LWP [b)].

(e.g. colder, warmer, polluted, clean, ocean, land) and comparing the outcomes to real data may help isolate the role of precipitation in pollution-cloud interactions. With respect to biomass burning, cloud modeling could help determine why the sensitivity of cloud optical depth was similar to droplet effective radius when biomass burning dominated pollution concentrations. For example, biomass burning plumes are known to contain dark carbonaceous molecules that are known to strongly absorb solar radiation both in the atmosphere (Brioude et al., 2009) and, when deposited, on the surface (McConnell et al., 2007). How this influences Arctic cloud evolution could be tested by simulating Arctic clouds, either polluted or clean, with an added cloud top radiative flux from a layer of biomass burning aerosols located above the cloud top. When the cloud model is able to replicate the observations, a better indication of the physical processes at play can be achieved.

Lastly, before variations in observed cloud properties can be firmly attributed to anthropogenic influence, a better characterization of how clouds influence and interact with the Arctic climate is needed. Long-term datasets of Arctic clouds do not exist due to the remoteness of the region. Also, satellite observations of the Arctic are generally often challenged by difficult meteorological conditions, such as an icy surface and temperature inversions (Liu and Key, 2003). Physical relationships between thermodynamic variables and cloud formation that have been developed in lower latitudes may not apply to similar clouds forming in the unique Arctic climate system (Klein and Hartmann, 1993; Curry, 1995; Pincus et al., 1997).

In particular, the physical processes governing phase transitions in clouds are not well understood. Mixed-phase stratiform clouds tend to form at temperatures well above the homogeneous freezing point of liquid water droplets, indicating the presence of sufficient supply of ice nuclei to support continuous ice crystal formation. Observations of Arctic aerosols during the wintertime have found that sulfuric acid coats the majority of large particles that typically act as ice nuclei (Curry, 1995). This inhibits freezing by water vapor deposition onto these large particles because the sulfuric acid reduces the freezing tem-

perature of the particle mixture, directly inhibiting one form of ice crystal generation, yet observations have found that low-level mixed-phase stratiform clouds can be maintained in a quasi-equilibrium state allowing droplet growth as well as continued ice crystal precipitation for days at a time (Intrieri et al., 2002; Shupe et al., 2006).

The analysis methods developed here could be applied to mixed-phase clouds to determine the sensitivity of cloud thermodynamic phase with respect to different parameters. For example, the effects of pollution on ice-crystal production potentially can be observed and quantified by analyzing the MODIS-POLDER phase index with co-located pollution tracer fields. Because the novel merged MODIS-POLDER phase retrieval includes a confidence index, a positive shift in the values of the index associated with lower pollution tracer concentrations (or vice versa) could indicate that pollution aerosols do infact inhibit ice crystal nucleation and growth. Furthermore, analyzing co-located droplet effective radius retrievals may indicate whether the reduced ice crystal growth is with respect to the aerosol indirect effect inhibiting riming processes (Morrison et al., 2008), or alternatively if no effect on droplet size is apparent ice nucleation may be inhibited by sulphuric acid droplets coalescing on ice nuclei (Curry, 1995; Girard et al., 2005).

Aircraft observations of Arctic clouds show that ice crystal concentrations are generally independent of temperature but closely related to the size of the largest liquid droplets contained in the cloud (Hobbs and Rangno, 1985). Potentially, by means of the aerosol indirect effect, additional CCN associated with polluted airmasses may indirectly extend the time of glaciation in mixed phase clouds. It has been demonstrated that the time needed for glaciation of mixed phase clouds is dependent on three fundamental variables, the vertical velocity, droplet number concentration and average droplet size (Korolev and Mazin, 2003). The vertical velocity is generally very weak in the Arctic lower troposphere (Curry et al., 1996, 1997; Shupe et al., 2006) making the latter two terms, number concentration and r_e , dominate in the time to glaciation, both of which can be inferred from satellite observations. Again, using the MODIS-POLDER phase retrieval and confidence index, the

dependence of cloud thermodynamic phase on these two parameters can be evaluated using space-based approach. Furthermore, the role of pollution on cloud phase transition can be tested by combing co-located pollution tracer measurements with cloud property retrievals from A-train.

The results presented in this thesis show a strong sensitivity of liquid low-level Arctic cloud properties to pollution. A natural extension would be to apply a similar analysis approach to analyze mixed-phase clouds. Physical processes influencing the mixed-phase cloud evolution are not well understood and given their prevalence and climatic importance, further study is warranted. Future work using combined pollution tracers and satellite cloud properties extended to mixed-phase clouds will further constrain important physical aspects governing cloud behaviour and evolution in the Arctic, potentially resolving some of the uncertainty involved with Arctic climate prediction.

REFERENCES

Ackerman, A. S., M. P. Kirkpatrick, D. E. Stevens, and O. B. Toon, 2004: The impact of humidity above stratiform clouds on indirect aerosol climate forcing. *Nature*, **432**, 1014–1017, doi:10.1038/nature03174.

Ackerman, A. S., O. B. Toon, and P. V. Hobbs, 1993: Dissipation of marine stratiform clouds and collapse of the marine boundary layer due to the depletion of cloud condensation nuclei by clouds. *Science*, **262**, 226–229, doi:doi:10.1126/science.262.5131.226.

Albrecht, B., 1989: Aerosols, cloud microphysics and fractional cloudiness. *Science*, **245**, 1227–1230, doi:10.1126/science.245.4923.1227.

Andreae, M. O., D. Rosenfeld, P. Artaxo, A. A. Costa, G. P. Frank, and K. M. Longo, 2004: Smoking Rain Clouds over the Amazon. *Science*, **303**, 1337–1342, doi:10.1126/science.1092779.

Avey, L., T. Garrett, and A. Stohl, 2007: Evaluation of the aerosol indirect effect using satellite, tracer transport model, and aircraft data from the international consortium for atmospheric research on transport and transformation. *J. Geophys. Res*, **112**, doi:10.1029/2006JD007581.

Baker, M. B. and R. J. Charlson, 1990: Bistability of CCN concentrations and thermodynamics in the cloud-topped boundary layer. *Nature*, **345**, doi:10.1038/345142a0.

Barrie, L. A., 1986: Arctic air pollution: An overview of current knowledge. *Atmos. Environ.*, **20**, 643–838.

Bigg, E. K. and C. Leck, 2001: Cloud-active particles over the central Arctic Ocean. *J. Geophys. Res.*, **106**, 32155–32166.

Bigg, E. K., C. Leck, and E. D. Nilsson, 1996: Sudden changes in arctic atmospheric aerosol concentrations during summer and autumn. *Tellus Series B Chemical and Physical Meteorology B*, **48**, 254–+, doi:10.1034/j.1600-0889.1996.t01-1-00009.x.

Bower, K. N. and T. W. Choularton, 1993: Cloud processing of the cloud condensation nucleus spectrum and its climatological consequences. *Q.J.R. Meteorol. Soc.*, **119**, 655–679, doi:10.1002/qj.49711951204.

Bréon, F., D. Tanré, and S. Generoso, 2002: Aerosol effect on cloud droplet size monitored from satellite. *Science*, **295**, 834–838, doi:10.1126/science.1066434.

Bréon, F. M. and S. Colzy, 1999: Cloud detection from spaceborne POLDER instrument and validation against surface synoptic observations. *J. Appl. Meteorol.*, **36**, 777–785, doi:10.1175/1520-0450.

Brioude, J., O. R. Cooper, G. Feingold, M. Trainer, S. R. Freitas, D. Kowal, J. Ayers, E. Prins, P. Minnis, S. A. McKeen, G. J. Frost, and E.-Y. Hsie, 2009: Effect of biomass burning on marine stratocumulus clouds off the California coast. *Atmos. Chem. Phys.*, **9**, 8841–8856, doi:10.5194/acp-9-8841-2009.

Buriez, J. C., C. Vanbauce, F. Parol, P. Goloub, M. Herman, B. Bonnel, Y. Fouquart, P. Couvert, and G. Seze, 1997: Cloud detection and derivation of cloud properties from polder. *Int. J. Rem. Sens.*, **18**, 2785–2813, doi:10.1080/014311697217332.

Chang, F. and J. A. Coakley, 2007: Relationships between Marine Stratus Cloud Optical Depth and Temperature Inferences from AVHRR Observations. *J. Climate*, **20**, 2022–2036, doi:10.1175/JCLI4115.1.

Costantino, L. and F. M. Bréon, 2010: Analysis of aerosol-cloud interaction from multi-sensor satellite observations. *Geophys. Res. Lett.*, **37**, 11801–+, doi:10.1029/2009GL041828.

Curry, J., W. Rossow, and D. Randall, 1996: Overview of Arctic cloud and radiation characteristics. *J. Climate*, **9**, 1731–1764, doi:10.1175/1520-0442(1996)009<1731:OOACAR>2.0.CO;2.

Curry, J. A., 1995: Interactions among aerosols, clouds and climate of the arctic ocean. *Sci. Total Environ.*, **9**, 1731–1764.

Curry, J. A., J. O. Pinto, T. Benner, and M. Tschudi, 1997: Evolution of the cloudy boundary layer during the autumnal freezing of the Beaufort Sea. *J. Geophys. Res.*, **102**, 13851–13860.

de Boer, G., E. W. Eloranta, and M. D. Shupe, 2009: Arctic Mixed-Phase Stratiform Cloud Properties from Multiple Years of Surface-Based Measurements at Two High-Latitude Locations. *J. Atmos. Sci.*, **66**, 2874–+, doi:10.1175/2009JAS3029.1.

Durkee, P. A., K. J. Noone, R. J. Ferek, D. W. Johnson, J. P. Taylor, T. J. Garrett, P. V. Hobbs, J. G. Hudson, C. S. Bretherton, G. Innis, G. M. Frick, W. A. Hoppel, C. D. AoDowd, L. M. Russell, R. Gasparovic, K. E. Nielsen, S. A. Tessmer, S. R. Osborne, R. C. Flagan, J. H. Seinfeld, and H. Rand, 2000: The impact of ship-produced aerosols on the microstructure and albedo of warm marine stratocumulus clouds: A test of MAST hypotheses 1 and 2. *J. Atmos. Sci.*, **57**, 2554–2569, doi:10.1175/1520-0469(2000)057<2554:TIOSPA>2.0.CO;2.

EMCWF, 2002: (P. W. White and Ed.) IFS documentation. Technical report, ECMWF, Reading, UK.

Feingold, G., 2003: Modeling of the first indirect effect: Analysis of measurement requirements. *Geophys. Res. Lett.*, **30**, doi:10.1029/2003GL017967.

Feingold, G., W. Eberhand, and D. E. Veron, 2003: First measurements of the Twomey indirect effect using ground based remote sensors. *Geophys. Res. Lett.*, **30**, doi:10.1029/2002GL016633.

Feingold, G., L. A. Remer, J. Ramaprasad, and Y. J. Kaufman, 2001: Analysis of smoke impact on clouds in Brazilian biomass burning regions: An extension of Twomey's approach. *J. Geophys. Res.*, **106**, 22907–22922, doi:10.1029/2001JD000732.

Ferek, G., D. A. Hegg, P. V. Hobbs, and P. E. Durkee, 1998: Measurements of ship-induced tracks in clouds off the washington coast. *J. Geophys. Res.*, **103**, doi:10.1029/98JD02121.

Ferek, R. J., T. Garrett, P. V. Hobbs, S. Strader, D. Johnson, J. P. Taylor, K. Nielsen, A. S. Ackerman, Y. Kogan, Q. Liu, B. A. Albrecht, and D. Babb, 2000: Drizzle suppression in ship tracks. *J. Atmos. Sci.*, **57**, 2707–2728, doi:10.1175/1520-0469(2000)057<2707:DSIST>2.0.CO;2.

Forster, C., A. Stohl, and P. Seibert, 2007: Parameterization of Convective Transport in a Lagrangian Particle Dispersion Model and Its Evaluation. *J. Appl. Meteorol.*, **46**, 403–+, doi:10.1175/JAM2470.1.

Fougnie, B., G. Bracco, B. Lafrance, C. Ruffel, O. Hagolle, and C. Tinel, 2007: PARASOL in-flight calibration and performance. *Appl. Opt.*, **46**, 5435–5451, doi:10.1364/AO.46.005435.

Fuelberg, H. E., D. L. Harrigan, and W. Sessions, 2010: A meteorological overview of the ARCTAS 2008 mission. *Atmos. Chem. Phys.*, **10**, 817–842, doi:10.5194/acp-10-817-2010.

Garrett, T. J., L. Avey, P. I. Palmer, A. Stohl, J. A. Neuman, C. A. Brock, T. Ryerson, and J. S. Holloway, 2006: Quantifying wet scavenging processes in aircraft observations of nitric acid and ccn. *J. Geophys. Res.*, **111**, doi:10.1029/2006JD007416.

Garrett, T. J., M. M. Maestas, S. K. Kruegar, and C. T. Schmidt, 2009: Accelerlation of a radiative-thermodynamic cloud feedback influencing arctic surface warming. *Geophys. Res. Lett.*, **36**, doi:10.1029/2009GL040195.

Garrett, T. J., L. F. Radke, and P. V. Hobbs, 2002: Aerosol Effects on Cloud Emissivity and Surface Longwave Heating in the Arctic. *J. Atmos. Sci.*, **59**, 769–778, doi:10.1175/1520-0469(2002)059.

Garrett, T. J. and C. Zhao, 2006: Increased arctic cloud longwave emissivity associated with pollution from mid-latitudes. *Nature*, **440**, 787–789, doi:10.1038/nature04636.

Garrett, T. J., C. Zhao, X. Dong., G. G. Mace, and P. V. Hobbs, 2004: Effects of varying aerosol regimes on low-level Arctic stratus. *Geophys. Res. Lett.*, **31**, doi:10.1029/2004GL019928.

Garrett, T. J., C. Zhao, and P. Novelli, 2010: Assessing the relative contributions of transport efficiency and scavenging to seasonal variability in arctic aerosol. *Tellus B.*, **62**, 190 – 196, doi:10.1111/j.1600-0889.2010.00453.x.

Giglio, L., J. Descloitres, C. O. Justice, and Y. J. Kaufman, 2003: An enhanced contextual fire detection algorithm for modis. *Remote Sensing of Environment*, **87**, 273 – 282, doi:DOI: 10.1016/S0034-4257(03)00184-6.

Girard, E., J.-P. Blanchet, and Y. Dubois, 2005: Effects of arctic sulphuric acid aerosols on wintertime low-level atmospheric ice crystals, humidity and temperature at alert, nunavut. *Atmospheric Research*, **73**, 131 – 148, doi:DOI: 10.1016/j.atmosres.2004.08.002.

Goloub, P., M. Herman, H. Chepfer, J. Riedi, G. Brogniez, P. Couvert, and G. Seze, 2000: Cloud thermodynamical phase classification from the POLDER spaceborne instrument. *J. Geophys. Res.*, **105**, 14747–14760, doi:10.1029/1999JD901183.

Han, Q., W. Rossow, J. Zeng, and R. Welch, 2002: Three different behaviours of liquid water path of water clouds in aerosol-cloud interactions. *J. Atmos. Sci.*, **59**, 726, doi:10.1175/1520-0469(2002)059<0726:TDBOLW>2.0.CO;2.

He, X., Y. Bai, D. Pan, Q. Zhu, and F. Gong, 2009: Cloud top height retrieval using polarizing remote sensing data of POLDER. *Atmos. Oceanic Sci. Lett.*, **2**, 73–78.

Hirdman, D., H. Sodemann, S. Eckhardt, J. F. Burkhart, A. Jefferson, T. Mefford, P. K. Quinn, S. Sharma, J. StrÃÂ¶m, and A. Stohl, 2010: Source identification of short-lived air pollutants in the arctic using statistical analysis of measurement data and particle dispersion model output. *Atmospheric Chemistry and Physics*, **10**, 669–693, doi:10.5194/acp-10-669-2010.

Hobbs, P. V., T. J. Garrett, R. J. Ferek, S. R. Strader, D. A. Hegg, G. M. Frick, W. A. Hoppel, R. F. Gasparovic, L. M. Russell, D. W. Johnson, C. O'Dowd, P. A. Durkee, K. E. Nielsen, and G. Innis, 2000: Emissions from Ships with respect to Their Effects on Clouds. *Journal of Atmospheric Sciences*, **57**, 2570–2590, doi:10.1175/1520-0469(2000)057<2570:EFSWRT>2.0.CO;2.

Hobbs, P. V. and A. L. Rangno, 1985: Ice particle concentrations in clouds. *J. Atmos. Sci.*, **42**, 2523–2549.

Holz, R. E., S. A. Ackerman, F. W. Nagle, R. Frey, S. Dutcher, R. E. Kuehn, M. A. Vaughan, and B. Baum, 2008: Global Moderate Resolution Imaging Spectroradiometer (MODIS) cloud detection and height evaluation using CALIOP. *J. Geophys. Res.*, **113**, 0–+, doi:10.1029/2008JD009837.

Intrieri, J. M., C. W. Fairall, M. D. Shupe, P. O. G. Persson, E. L. Andreas, P. S. Guest, and R. E. Moritz, 2002: An annual cycle of arctic surface forcing at SHEBA. *J. Geophys. Res.*, **107**.

Jacob, D. J., J. H. Crawford, A. D. Clarke, J. E. Dibb, L. K. Emmons, R. A. Ferrare, C. A. Hostetler, P. B. Russell, H. B. Singh, A. M. Thompson, G. E. Shaw, E. McCauley, J. R. Pederson, and F. J. A., 2010: The Arctic Research of the Composition of the Troposphere from Aircraft and Satellites (ARCTAS) mission: design, execution, and first results. *Atmos. Chem. Phys. Discuss.*, **10**, 5191–5212.

Kato, S., N. Loeb, P. Minnis, J. Francis, and T. Charlock, 2006: Seasonal and interannual variations of top-of-atmosphere irradiance and cloud cover over polar regions derived from the ceres data set. *Geophys. Res. Lett.*, **33**.

Kaufman, Y., I. Koren, L. Remer, D. Rosenfeld, and Y. Rudich, 2005: The effect of smoke, dust, and pollution aerosol on shallow cloud development over the atlantic ocean. *Proc. Natl. Acad. Sci.*, **102**, doi:10.1073/pnas.0505191102.

Kawamoto, K., T. Hayasaka, I. Uno, and T. Ohara, 2006: A correlative study on the relationship between modeled anthropogenic aerosol concentration and satellite-observed cloud properties over east Asia. *J. Geophys. Res.*, **111**, doi:10.1029/2005JD006919.

King, M. D., S. Platnick, D. Kaufman, B. C. Tanre, W. P. Menzel, L. A. Remer, S. A. Ackerman, and S. Gao, 2003: Cloud and aerosol properties, precipitable water, and profiles of temperature and humidity from modis. *IEEE, Trans. Geosci. Remote Sensing*, **41**, 442–458.

King, M. D., S. E. Platnick, P. A. Hubanks, T. G. Arnold, and B. Wind, 2005: Collection 005 Change Summary for the MODIS Cloud Optical Property Algorithm. *NASA Tech Report*.

King, M. D., L. F. Radke, and P. V. Hobbs, 1993: Optical properties of marine stratocumulus clouds modified by ships. *J. Geophys. Res.*, **98**, 2729.

Klein, S. A. and D. L. Hartmann, 1993: The seasonal cycle of low stratiform clouds. *J. Climate*, **6**, 1587–1606, doi:10.1175/1520-0442(1993)006<1587:TSCOLS>2.0.CO;2.

Korolev, A. V. and I. P. Mazin, 2003: Supersaturation of water vapor in clouds. *J. Atmos. Sci.*, **60**, 2957–2974.

Kubar, T., D. L. Hartmann, and R. Wood, 2009: Understanding the importance of microphysics and macrophysics for warm rain in marine low clouds. $PartI : SatelliteObservations$. *J. Atmos. Sci.*, **66**, 2953+–, doi:10.1175/2009JAS3071.1.

Law, K. S. and A. Stohl, 2007: Arctic air pollution: Origins and impacts. *Science*, **315**, doi:10.1126/science.1137695.

Lihavainen, H., V. M. Kerminen, and L. A. Remer, 2009: Aerosol-cloud interaction determined by both in situ and satellite data over a northern high-latitude site. *Atmos. Chem. Phys. Discuss.*, **9**.

Liu, Y. and J. R. Key, 2003: Detection and Analysis of Clear-Sky, Low-Level Atmospheric Temperature Inversions with MODIS. *Journal of Atmospheric and Oceanic Technology*, **20**, 1727–+, doi:10.1175/1520-0426(2003)020<1727:DAAOCL>2.0.CO;2.

Lohmann, U. and J. Feichter, 2005: Global indirect aerosol effects: a review. *Atmos. Chem. Phys.*, 715–737, doi:1680-7324/acp/2005-5-715.

Longley, I., D. Inglis, M. Gallagher, P. Williams, and J. Allen, 2005: Using NOx and CO monitoring data to indicate fine aerosol number concentrations and emissions factors in three UK conurbations. *Atmos. Environ.*, **39**, 5157 – 5169, doi:10.1016/j.atmosenv.2005.05.017.

Lu, M. L. and J. H. Seinfeld, 2005: Study of the aerosol indirect effect by large-eddy simulation of marine stratocumulus. *J. Atmos. Sci.*, **62**, 3909–3932, doi:10.1175/JAS3584.1.

Lubin, D. and A. M. Vogelmann, 2006: A climatologically significant aerosol longwave indirect effect in the arctic. *Nature*, **439**, 453–456, doi:10.1038/nature04449.

— 2007: Expected magnitude of the aerosol shortwave indirect effect in springtime arctic liquid water clouds. *Geophys. Res. Lett.*, **34**, 11801.

Mauger, G. S. and J. R. Norris, 2007: Meteorological bias in satellite estimates of aerosol-cloud relationships. *Geophys. Res. Lett.*, **34**, 16824–+, doi:10.1029/2007GL029952.

Mauritsen, T., J. Sedlar, M. Tjernström, C. Leck, M. Martin, M. Shupe, S. Sjogren, B. Sierau, P. O. G. Persson, I. M. Brooks, and E. Swietlicki, 2010: Aerosols indirectly warm the Arctic. *Atmos. Chem. Phys. Discuss.*, **10**, 16775–16796, doi:10.5194/acpd-10-16775-2010.

McConnell, J. R., R. Edwards, G. L. Kok, M. G. Flanner, C. S. Zender, E. S. Saltzman, R. Banta, D. R. Pasteris, M. M. Carter, and J. D. W. Kahl, 2007: 20th-century industrial black carbon emissions altered arctic climate forcing. *Sciencexpress*.

Morrison, H. and J. O. Pinto, 2005: Mesoscale modeling of springtime arctic mixed-phase stratiform clouds using a new two-moment bulk microphysics scheme. *J. Atmos. Sci.*, **62**, 3683–3704, doi:10.1175/JAS3564.1.

Morrison, H., O. J. Pinto, J. A. Curry, and G. M. McFarquhar, 2008: Sensitivity of modeled arctic mixed-phase stratocumulus to cloud condensation and ice nuclei over regionally varying surface conditions. *J. Geophys. Res.*, **113**, doi:10.1029/2007JD008729.

Myhre, G., F. Stordal, M. Johnsrud, Y. J. Kaufman, D. Rosenfeld, T. Storelvmo, J. E. Kristjansson, T. K. Berntsen, A. Myhre, and I. S. A. Isaksen, 2007: Aerosol-cloud interaction inferred from MODIS satellite data and global aerosol models. *Atmos. Chem. Phys.*, **7**, 3081–3101, doi:10.5194/acp-7-3081-2007.

Nakajima, T., A. Higurashi, and J. E. Penner, 2001: A possible correlation between satellite-derived cloud and aerosol microphysical parameters. *Geophys. Res. Lett.*, **28**, doi:10.1029/2000GL012186.

Olivier, J. G. and J. J. M. Berdowski, 2001: Global emission sources and sinks in: Berdowski, J., Guicherit, R. and B.J. Heij (eds.) "The Climate System". Technical report, A. A. Balkema Publishers Swets Zeitlinger Publishers, Lisse, The Netherlands.

Paris, J., P. Ciais, P. Nédélec, M. Ramonet, B. D. Belan, M. Y. Arshinov, G. S. Golitsyn, I. Granberg, A. Stohl, G. Cayez, G. Athier, F. Boumard, and J. M. Cousin, 2008: The YAK-AEROSIB transcontinental aircraft campaigns: new insights on the transport of $CO_2, CO and O_3$ across Siberia. *Tellus B.*, **60**, 551–568, doi:10.1111/j.1600-0889.2008.00369.x.

Paris, J. D., A. Stohl, P. Nédélec, M. Y. Arshinov, M. V. Panchenko, V. P. Shmargunov, K. S. Law, B. D. Belan, and P. Ciais, 2009: Wildfire smoke in the siberian arctic in summer: source characterization and plume evolution from airborne measurements. *Atmospheric Chemistry and Physics*, **9**, 18201.

Pincus, R., M. B. Baker, and C. S. Bretherton, 1997: What Controls Stratocumulus Radiative Properties? Lagrangian Observations of Cloud Evolution. *Journal of Atmospheric Sciences*, **54**, 2215–2236, doi:10.1175/1520-0469(1997)054<2215.

Platnick, S., M. D. King, S. A. Ackerman, and J. Riedi, 2003: The MODIS Cloud Products: Algorithms and Examples From Terra. *IEEE, Trans. Geosci. Remote Sensing*, **41**, 459 – 473, doi:10.1109/TGRS.2002.808301.

Pradeep Kumar, P., K. Broekhuizen, and J. P. D. Abbatt, 2003: Organic acids as cloud condensation nuclei: Laboratory studies of highly soluble and insoluble species. *Atmos. Chem. and Phys.*, **3**, 509–520.

Quinn, P. K., T. S. Bates, E. Baum, N. Doubleday, A. M. Fiore, M. G. Flanner, T. J. Garrett, and D. Koch, 2008: Short-lived pollutants in the Arctic: their climate impact and possible mitigation strategies. *Atmos. Chem. Phys.*, **8**, 1723–1735, doi:10.5194/acp-8-1723-2008.

Quinn, P. K., G. Shaw, E. Andrews, E. G. Dutton, T. Ruoho-Airola, and S. L. Gong, 2007: Arctic haze: current trends and knowledge gaps. *Tellus B.*, **59**, 99–114, doi:10.1111/j.1600-0889.2006.00238.x.

Radke, L. F., J. A. Coakley, and M. D. King, 1989: Direct and remote sensing of observations of the effects of ships on clouds. *Science*, **246**, 1146, doi:10.1126/science.246.4934.1146.

Riedi, J., B. Marchant, S. Platnick, B. Baum, F. Thieuleux, C. Oudard, F. Parol, J. Nicolas, and P. Dubuisson, 2007: Cloud thermodynamic phase inferred from merged POLDER and MODIS data. *Atmos. Chem. Phys. Discuss.*, **7**, 14103–14137, doi:16807367.

Rivera-Carpio, C. A., C. E. Corrigan, T. Novakov, J. E. Penner, C. F. Rogers, and J. C. Chow, 1996: Derivation of contributions of sulfate and carbonaceous aerosols to cloud condensation nuclei from mass size distributions. *J. Geophys. Res.*, **101**, 19483–19494, doi:10.1029/95JD01077.

Rosenfeld, D. and G. Feingold, 2003: Explanation of discrepancies among satellite observations of the aerosol indirect effects. *Geophys. Res. Lett.*, **30**, 1776, doi:10.1029/2003GL017684.

Schwartz, S., A. Harshvardham, and C. Benkovitz, 2002: Influence of anthropogenic aerosol on cloud optical depth and albedo shown by satellite measurements and chemical transport modeling.

Sekiguchi, M., T. Nakajima, K. Suzuki, K. Kawamoto, and D. Rosenfeld, 2003: A study of the direct and indirect effects of aerosols using global satellite data sets of aerosol and cloud parameters. *J. Geophys. Res.*, **108**, doi:10.1029/2002JD003359.

Shaw, P. M., L. M. Russell, A. Jefferson, and P. K. Quinn, 2010: Arctic organic aerosol measurements show particles from mixed combustion in spring haze and from frost flowers in winter. *J. Geophys. Res.*, **37**, 10803–+, doi:10.1029/2010GL042831.

Shindell, D. and G. Faluvegi, 2009: Climate response to regional radiative forcing during the twentieth century. *Nature*, **2**, 294–300, doi:10.1038/ngeo473.

Shupe, M. D., S. Y. Matrosov, and T. Uttal, 2006: Arctic mixed-phase cloud properties derived from surface-based sensors at SHEBA. *J. Atmos. Sci.*, **63**, 697–711, doi:10.1175/JAS3659.1.

Solomon, S., D. Qin, M. Manning, Z. Chen, K. Averyt, M. Tignor, and H. L. Miller, 2007: *Intergovernmental Panel on Climate Change, Climate Change 2007 - The Physical Science Basis Contribution of Working Group I to the Fourth Assessment Report of the Intergovernmental Panel on Climate Change*. Cambridge University Press.

Stephens, G. and a. et, 2002: The CloudSat mission and the A-Train: A new dimension of spacebased observations of clouds and precipitation. *Bull. Amer. Meteor. Soc.*, **83**, 1771–1790, doi:10.1175/BAMS-83-12-1771.

Stevens, B. and G. Feingold, 2009: Untangling aerosol effects on clouds and precipitation in a buffered system. *Nature*, **461**, 607–613, doi:10.1038/nature08281.

Stohl, A., 2006: Characteristics of atmospheric transport into the arctic troposphere. *J. Geophys. Res.*, **111**, 11306–+.

Stohl, A., E. Andrews, J. F. Burkhart, C. Forster, A. Herber, S. W. Hoch, D. Kowal, C. Lunder, T. Mefford, J. A. Ogren, S. Sharma, N. Spichtinger, K. Stebel, R. Stone, J. Ström, K. Tørseth, C. Wehrli, and K. E. Yttri, 2006: Pan-Arctic enhancements of light absorbing aerosol concentrations due to North American boreal forest fires during summer 2004. *J. Geophys. Res.*, **111**, 22214–+, doi:10.1029/2006JD007216.

Stohl, A., T. Berg, J. F. Burkhart, C. Forster, A. Herber, C. Lunder, W. McMillan, S. Oltmans, M. Shiobara, D. Simpson, S. Solberg, K. Stebel, J. Strom, R. Treffeisen, K. Virkkunen, and K. E. Yttri, 2007: Arctic smoke - record high air pollution levels in the european arctic due to agricultural fires in eastern europe in spring 2006. *Atmos. Chem. Phys.*, **7**, 511–534.

Stohl, A., C. Forster, A. Frank, and P. Seibert, 2005: Technical note: The lagrangian particle dispersion model flexpart version 6.2. Technical report, NILU.

Stohl, A., M. Hittenberger, and G. Wotawa, 1998: Validation of the lagrangian particle dispersion model FLEXPART against large-scale tracer experiment data. *Atmos. Environ.*, **32**, 4245 – 4264, doi:DOI: 10.1016/S1352-2310(98)00184-8.

Stohl, A. and D. J. Thomson, 1999: A Density Correction for Lagrangian Particle Dispersion Models. *Bound.-Lay. Meteorol.*, **90**, 155–167, doi:10.1023/A:1001741110696.

Twomey, S., 1977: The influence of pollution on the shortwave albedo of clouds. *J. Atmos. Sci.*, **34**, 1149–1154, doi:10.1175/1520-0469(1977)034<1149:TIOPOT>2.0.CO;2.

Vavrus, S., 2004: The impact of cloud feedbacks on arctic climate under greenhouse forcing. *J. Climate*, **17**, 603–615.

Vestin, A., J. Rissler, E. Swietlicki, G. P. Frank, and M. O. Andreae, 2007: Cloud-nucleating properties of the Amazonian biomass burning aerosol: Cloud condensation nuclei measurements and modeling. *J. Geophys. Res.*, **112**, 14201–+, doi:10.1029/2006JD008104.

Warneke, C., R. Bahreini, J. Brioude, C. A. Brock, J. A. de Gouw, D. W. Fahey, K. D. Froyd, J. S. Holloway, A. Middlebrook, L. Miller, S. Montzka, D. Murphy, J. Peischl, T. B. Ryerson, J. Schwarz, J. R. Spackman, and P. Veres, 2009: Biomass burning in Siberia and Kazakhstan as an important source for haze over the Alaskan Arctic in April 2008. *Geophys. Res. Lett.*, **36**, doi:10.1029/2008GL036194.

Warneke, C., K. D. Froyd, J. Briode, and A. Stohl, 2010: An important contribution to springtime Arctic aerosol from biomass burning in Russia. *Geophys. Res. Lett.*, **37**, doi:10.1029/2009GL041816.

Weisz, E., J. Li, W. P. Menzel, A. K. Heidinger, and B. H. Kahn, 2007: Comparison of AIRS, MODIS, CloudSat and CALIPSO cloud top height retrievals. *Geophys. Res. Lett.*, **34**, doi:10.1029/2007GL030676.

Winker, D. M., M. A. Vaughan, A. Omar, Y. Hu, K. A. Powell, Z. Liu, W. H. Hunt, and S. A. Young, 2009: Overview of the CALIPSO Mission and CALIOP Data Processing Algorithms. *J. Atmos. Oceanic Technol.*, **26**, 2310–+, doi:10.1175/2009JTECHA1281.1.

Winton, M., 2006: Amplified arctic climate change: What does surface albedo feedback have to do with it? *Geophys. Res. Lett.*, **33**.

Wood, R., 2007: Cancellation of aerosol indirect effects in marine stratocumulus through cloud thinning. *J. Atmos. Sci.*, **64**, 2657–2669, doi:10.1175/JAS3942.1.

Wylie, D. P. and J. G. Hudson, 2002: Effects of long-range transport and clouds on cloud condensation nuclei in the springtime arctic. *J. Geophys. Res.*, **107**, doi:10.1029/2001JD000759.

Xue, H. and G. Feingold, 2006: Large eddy simulations of trade wind cumuli: Investigation of aerosol indirect effects. *J. Atmos. Sci.*, 1605–1622, doi:10.1175/JAS3706.1.

Yao, Z., Z. Han, Z. Zhao, L. Lin, and X. Fan, 2010: Synergetic use of POLDER and MODIS for multilayered cloud identification. *J. Rem. Sens. Env.*, **114**, 1910–1923, doi:10.1016/j.rse.2010.03.014.